6-1-2019

Cobalt Sulfide/Spongy functionalized Graphene nanostructured electrodes for High-Performance Supercapacitors

Israa Mohamed Afifi

American University in Cairo

School of Sciences and Engineering

Physics Department

Cobalt Sulfide/Spongy functionalized Graphene nanostructured electrodes for High-Performance Supercapacitors

A thesis submitted in partial fulfilment of the requirements for the degree of Master of Science in Physics

By

Israa Mohamed Afifi

Supervised by

Dr. Nageh Allam

Acknowledgement

It is an absolute pleasure to express my deepest gratitude and sincere appreciation to my mentor, Dr. Nageh Allam. Thank you for giving me the honour and opportunity of being a part of EML lab, and much gratitude to the endless effort, guidance and patience. Deepest appreciation for being very nice to me and keeping your door open to me and everyone.

I wish to express my sincere appreciation to my colleague Dr. Dalia El Gendy for her endless help and efforts.

I would like to express my genuine gratitude to all my colleagues in EML lab for being very helpful.

My sincere appreciation to all my professors and colleagues in the physics department.

I would like to take a moment to thank my family: My mother, father, sister and husband for the endless support.

Finally, I would like to express my sincere appreciation to all those who helped me making it possible to complete this work in its final form.

Dedication

To my Son, Yassin.

Abstract

A simple approach is illustrated for the preparation of functionalized spongy graphene/cobalt sulfide (FG-CoS) nanocomposites as unified, porous 3-dimensional (3D) network crinkly sheets. These crinkly sheets contain the reduced spongy graphene oxide (SGO) sheets and the intercalated CoS nanoparticles within the spongy graphene. The fabricated FG-CoS composites were characterized by X-ray diffraction (XRD), scanning electron microscopy (SEM), Fourier-transform infrared spectroscopy (FTIR), and Raman spectroscopy. The synthesized materials were examined as supercapacitor materials in an aqueous electrolyte (3M KOH) using cyclic voltammetry (CV) at a wide range of potential scan rates, and galvanostatic charge/discharge at various current densities. The FG-CoS electrode yielded a maximum specific capacitance of 1072 F/g at a scan rate of 1 mV/s. In addition, it showed outstanding cyclability retention of 117% after the 1000^{th} cycle at 100mV/s. The obtained energy density is 35.2 Wh/kg along with a power density of 250 W/kg at 1.0 A/g. Such high performance can be attributed to the synergistic effect of graphene and CoS, where CoS is sandwiched between graphene nanosheets. This makes the FG/CoS composite a promising electrode material for a superior-performance supercapacitor.

Table of Contents

Chapter 1: Introduction and scope of work……1

1.1 Necessity for energy storage ……..…1

1.2 Supercapacitors……..…….…….…2

1.3 Aim of work……...…….....…5

References…….....6

Chapter 2: Theoretical background…….....….7

2.1 Electrostatic capacitors Vs. Supercapacitors……...7

2.2 Batteries, Fuel cells and Supercapacitors……..……..9

2.2.1 Batteries Vs. fuel cells Vs. electrochemical supercapacitors……..... 9

2.2.2 Ragone Plot……...10

2.2.3 Kinetics of an electrochemical system…….....10

2.3 Classification of supercapacitors…….....12

2.3.1 Electrochemical double-layer supercapacitors…….13

2.3.1.1 Diffuse layer…….14

2.4 Calculations…….....15

2.4.1 Specific capacitance…….…….15

2.4.2 Energy density…….…..16

2.4.3 ESR (equivalent series resistance) ……...16

2.4.4 Power density……....17

2.5 Pseudocapacitors…….....17

2.5.1 Basic electrochemistry of pseudocapacitors……..18

2.6 Hybrid supercapacitors…….…..…19

2.6.1 Asymmetric hybrid supercapacitor…….……...20

2.6.2 Symmetric hybrid supercapacitors…….20

2.6.3 Battery-like supercapacitors……...20

2.7 Applications of Supercapacitors…….20

2.8 Components for supercapacitors……..…21

2.8.1 Electrode requirements for supercapacitors……...…21

2.8.1.1 Electrical conductivity of the electrode material……..…22

2.8.1.2 High specific surface area……22

2.8.2 Current collectors…….....23

2.8.3 Separators……..…23

2.8.4 Electrolytes……24

2.8.4.1 Aqueous electrolytes……24

2.8.4.2 Organic electrolytes…….....25

2.8.4.3 Ionic liquids…….…26

2.8.4.4 Solid-state polymer electrolytes……..26

References……..……27

Chapter 3: Literature Review……..……32

3.1 Introduction……32

3.1.1 Graphite and Graphene……...…32

3.2 Preparation of graphene……...……...33

3.2.1 Chemical Vapour Deposition……...…..…33

3.2.2 Epitaxial growth on metal surfaces……..…….....…33

3.2.3 Mechanical Exfoliation……..……34

3.2.4 Liquid phase exfoliation…….....…34

3.2.5 Hummer's method……..……36

3.3 Reduction strategies of Graphene oxide……..……..…36

3.3.1 Thermal Annealing……..……..……...…….36

3.3.2 Chemical Reduction……..……..37

3.3.2.1 Chemical reagent reduction……..……...…..…37

3.3.2.2 Reduction by Hydrazine……..38

3.3.2.3 Reduction using metal hydrides……...38

3.4 Reduction mechanism……38

3.5 Reduced graphene oxide as supercapacitor's electrode material……...…39

3.6 Activated graphene oxide as a supercapacitor electrode material…….…....42

3.6.1 Functionalization with polymers…….……42

3.6.2 Functionalization with Nano particles…….……42

3.6.3 Functionalization with organic compounds…….…….43

3.7 Graphene/Metal oxides composite electrode materials……..……44

3.7.1 Graphene/Ruthenium oxide-based electrode materials…….……45

3.7.2 Graphene/Manganese oxide-based electrode materials…….…….46

3.7.3 Graphene/Cobalt oxide-based electrode materials…….....46

3.8 Graphene /metal sulphides-based electrode materials……...…47

3.9 Metal oxides used as supercapacitor electrodes……..….48

3 .10 Metal sulphides used as electrode materials……...50

References…….51

Chapter 4: Materials and Methods…….61

4.1 Materials…….…..……61

4.2 Synthesis and fabrication……..…..61

4.2.1 spongy graphene oxide (SGO) synthesis……..……...61

4.2.2 Adenine-functionalized graphene oxide preparation……...…..62

4.2.3 Preparation of CoS and functionalized graphene (FG-COS) Powder……...….62

4.2.4 Electrodes preparation and electrochemical measurements……..…....64

4.3 Characterization techniques…….64

4.3.1 Physical Characterization……...64

4.3.1.1 Crystallinity……64

4.3.1.2 Morphology……..…….....65

4.3.1.3 Composition…….…67

4.3.2 Electrochemical Characterization……67

4.3.2.1 Cyclic Voltammetry……..67

4.3.2.2 Galvanostatic charge/discharge…….68

4.3.3.3 Cycle life measurement using Charging-Discharging curves……...……68

References……69

Chapter 5: Results and Discussion……...…69

5.1 Physical Characterization…….……69

5.1.1 Surface morphology (FESEM)……69

5.1.2 Crystallinity (XRD)…….……72

5.1.3 Composition, Morphology and Chemical structure…….72

5.2 Electrochemical characterization……75

5.2.1 Cyclic Voltammetry measurements……75

5.2.2 Galvanostatic charge/discharge……...…77

5.2.3 Energy and power density……79

References……82

Chapter 6: Conclusion and Future work……...…85

6.1 Conclusion……85

6.2 Future work…….85

List of Figures

Fig. 1.1: Applications of electrochemical capacitors.[1] ……..……1

Fig. 1.2: Electrochemical Double Layer Capacitors.[4] ……. …...……..…2

Fig 1.3: Schematic diagram of (a) electrical double-layer capacitor (EDLC), (b) pseudocapacitors (PC) and (c)hybrid supercapacitor (HSC)

carbon-based supercapacitors for efficient energy storage.[8] ……..……..…....4

Fig.2.1: Schematic diagram of a charged capacitor.[2]……..…….…...7

Fig 2.2: Ragone plot. [6]…….….10

Fig 2.3: Schematic diagram of a discharge curve of a battery[5] ……..……..12

Fig 2.4: Classification of supercapacitors. [2]……12

Fig 2.5: Electric double-layer supercapacitor [48]……..14

Fig.2.6: Double-layer models at interface of electrode and electrolyte solution. [49,…]..15

Fig.2.7: Applications of Supercapacitors.[30] ……..…...20

Fig 2.8: Effect of pore size on supercapacitor ‘s specific surface area. [49] ……22

Fig.2.9: Ceramic-based separators. [38] …….....23

Fig.2.10: Classification of electrolytes reference. [39] ……..…..24

Fig 3.1: 0D buckyballs, 1D nanotubes and 3D graphene. [4]…….……....32

Fig 3.2: Schematic diagram of Si sublimation [10]…….……..34

Fig 3.3: Process of Graphene exfoliation. [8]……..35

Fig 3.4: Graphite, graphite and graphene oxide difference in structure. [26]…….....36

Fig 3.5: effect of increasing annealing temperature of reduced graphene oxide on the electrical conductivity. [16]……...37

Fig 4.1: Scheme of Synthesis of CoS and FG-CoS ……63

Fig 4.2:Modern X-ray diffractometer. (Courtesy of Panalytics, XPert Powder). [5]……....65

Fig 4.3:Materials Characterization Using (NDE) Methods.[7]…….…....66

Figure 5.1: FESEM Images of (a) spongy SGO, (b) CoS, (c) FG-CoS, and (d) EDX spectra of the FG-CoS nanocomposite…….…….71

Figure 5.2:. (a) XRD pattern, (b) FTIR spectra, and (c) Raman spectra of the fabricated materials…….…..74

Figure 5.3: (a) Cyclic voltammograms of FG-CoS and SGO electrodes in 3 M KOH at a scan rate of 5 mV/s, (b) cyclic voltammograms of FG-CoS electrodes at different scan rates, and (c) Specific capacitance of FG-CoS electrodes at various scan rates in 3 M KOH…….…….76

Figure 5.4: . (a) Galvanostatic charge/discharge, (b) variation of specific capacitance with current density, (c) the first and 1000thCV cycles of the FG-CoS electrodes, and (d) Ragone plot at different current densities……80

List of Tables

Table 2.1: Electrolyte resistance and voltage of various aqueous electrolytes. [42]…..…25

Table 2.2: Relation between pore size, capacitance and internal resistance. [45] ……26

Table 5.1: Specific capacitances of doped graphene compared to our work…….79

Table 5.2: Ragone table for reported energy and power density values compared to our work…….82

Chapter 1: Introduction

1.1 Necessity for energy storage

In the present energy –dependent world, fast industrialization and development of the worldwide human populace have depleted the world's energy resources. For centuries, communities have been relying on conventional energy sources, such as fossil fuels. Those conventional energy resources as well as being non-sustainable are elements of air pollution and global warming. Owing to this, the search for alternative energy sources and storage devices is fundamental. The solar cell ingests energy from the sun early in the day; nonetheless, they cannot store it for additionally utilize. In this context research for alternative storage/ conversion devices is essential. Fuel cells, batteries and supercapacitors are front lines of electrochemical storage systems. Electrochemical storage (EECS) can be incorporated with the sun powered cell as a capacity gadget in the form of batteries or supercapacitors. The aim of those devices is to hold enough capacities to store the energy outfit by numerous applications.

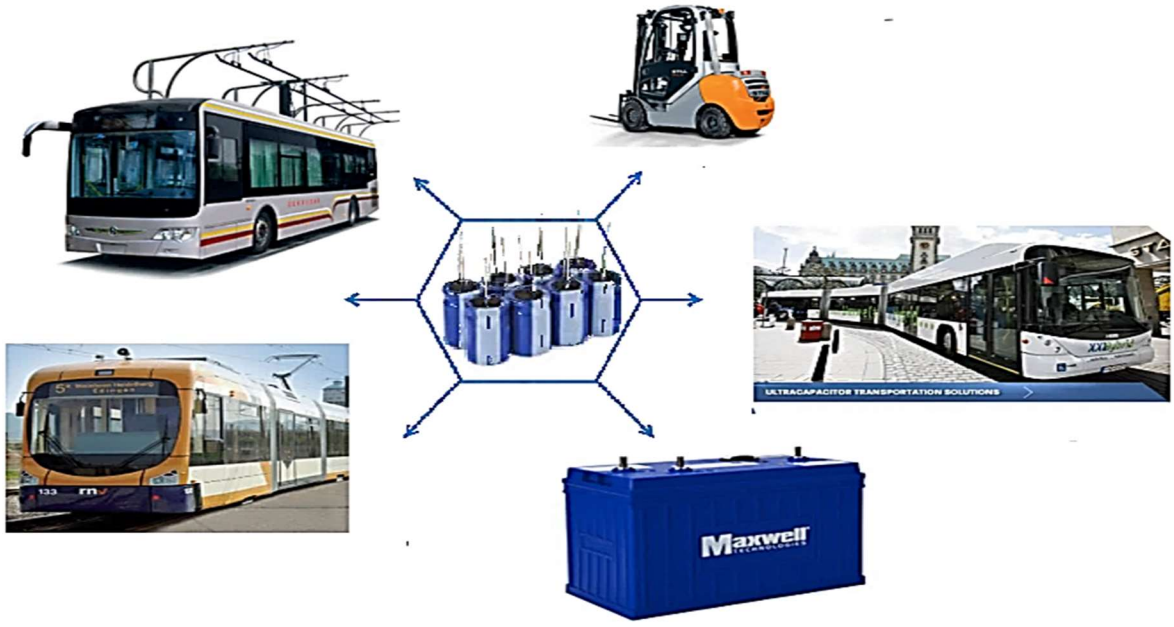

Fig. 1.1: Applications of electrochemical capacitors. (1).

1.2 Supercapacitors

Electrochemical supercapacitors (ES), also called supercapacitors, electrical double layer capacitors (EDLS) or ultra-supercapacitors, possess high power density and life cycle compared to batteries and high energy density compared to normal dielectric capacitors. In addition to this, supercapacitors are distinguished by the long charge-discharge life cycles, and wide working temperature ranges. (2).

An electrochemical supercapacitor (ES) consists of two electrodes, an electrolyte and a separator that helps isolating the electrodes. ES can be classified into two main types according to charge storage mechanism: electrochemical double layer supercapacitor (EDLCS), pseudocapacitors, or sometimes referred to as faradic supercapacitors. In case of EDLCS, charge storage mechanism is via adsorption of ions on the electrolyte- electrode interface due to coulomb's force. i.e. it is the electrostatic mechanism that governs the charge transfer. The electric double layer is formed due to the charge balance between the electrolyte and the electrode. For pseudocapacitors, electrochemically active materials cause faradic charge transfer in the electrode porous layer. Such charge transfer is kinetically and thermodynamically driven redox reactions (3).

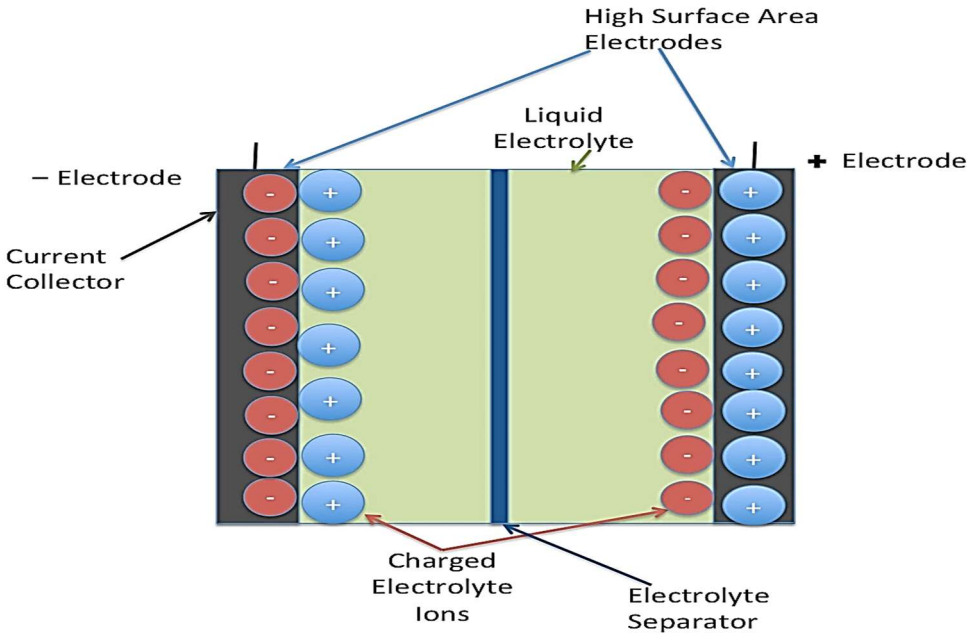

Fig.1.2: Electrochemical Double Layer Capacitors (4)

Electric double layers have a similar nature of that of conventional physical batteries, as charge storage mechanism is physical. Such storage mechanism occurs at the electrode / electrolyte interface. Even though Double layer capacitors are characterized by the relatively long-life cycles, their capacitance values are low, since it depends only on the active surface area contributing to adsorption. Electrode materials used in EDLCS are mainly carbon- based materials with high specific surface area. such high specific surface area makes carbon materials ideal for EDLS in terms of specific power and life cycle. Unluckily, the contact resistance between carbon atoms leads to high resistivity, which results in decreasing conductivity. (5,6).Pseudocapacitors materials such as transition metal oxides and conducting polymers, yield high energy density due to the redox reactions. They are known for their high capacitance than EDLCS, but material degradation is their major drawback. (7).

Hybrid supercapacitors are another kind of supercapacitors, which comprises of at least two materials. (e.g. nano– materials carbon nanotubes with conducting polymers as well as metal oxides). EDLC carbon materials alone regularly have constrained specific capacitance, while pseudocapacitive materials alone have higher specific capacitance however poor conductivity. In this manner, there is a requirement for devices comprising of carbon with pseudo capacitive materials as composite or asymmetric supercapacitors, to get elite anode materials that can be utilized as a part of superior supercapacitors. (8).

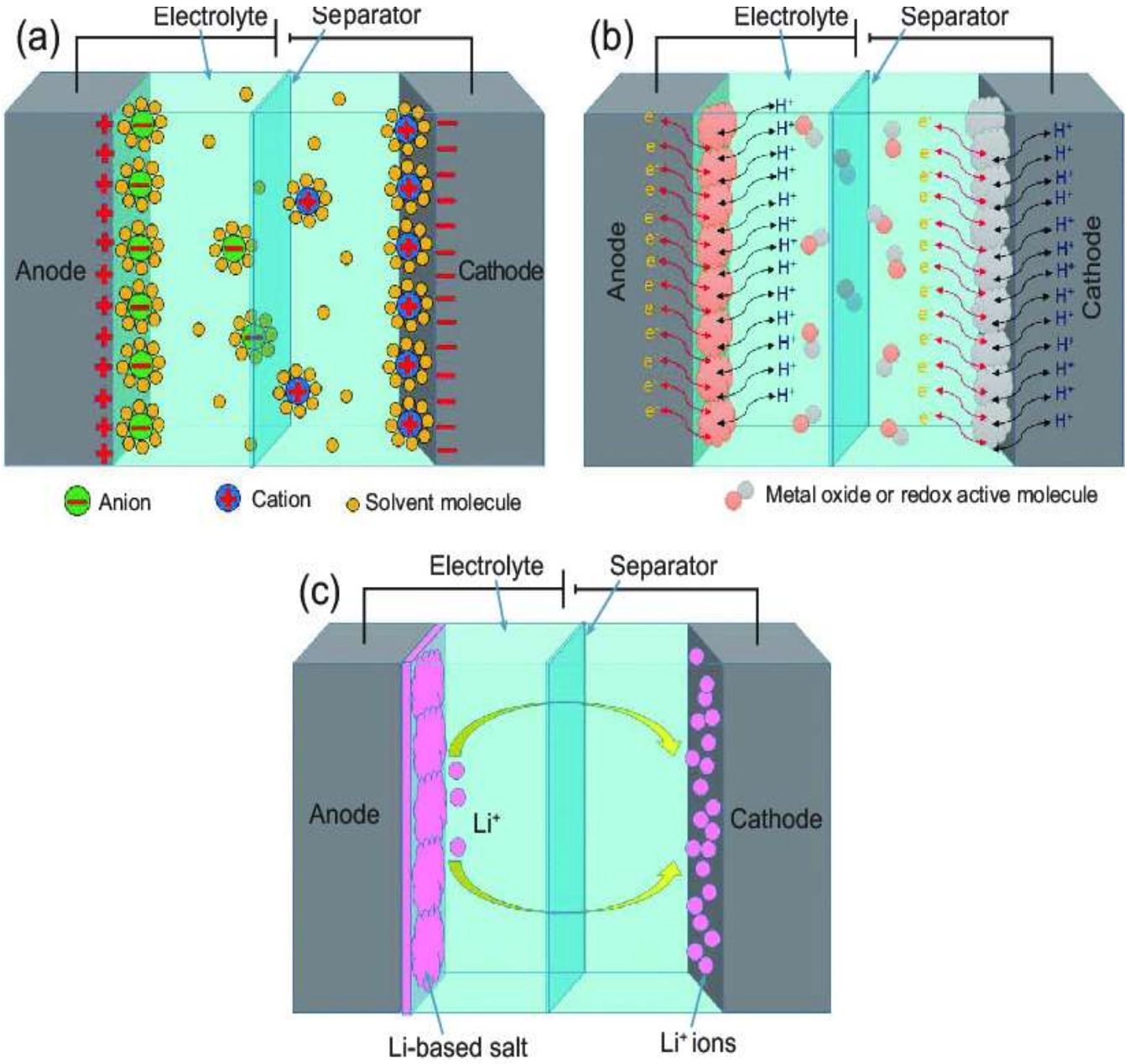

Fig.1.3: Schematic diagram of (a) electrical double-layer capacitor (EDLC), (b) pseudocapacitors (PC) and (c) hybrid supercapacitor (HSC). Carbon-based supercapacitors for efficient energy storage. (8)

1.3 Aim of work

The presented thesis aims at (1) preparing functionalized spongy graphene/cobalt sulfide (FG-CoS) nanocomposites as electrode materials for supercapacitors using easy and eco-friendly methods.(2) characterize functionalized spongy graphene/cobalt sulfide (FG-CoS) nanocomposites as electrode material for supercapacitors that would further enhance the performance of a supercapacitor's life time, power density, energy density and cyclability.

The proposal of using metal sulphides along with graphene-based materials is to combine figures of merit of both. Regarding metal sulphides, they possess pseudocapacitance behaviour and presence of two or more oxidation states. The high theoretical capacity of Sulphur compounds provides excellent capacitance behaviour and makes it an excellent candidate to be used in supercapacitors. On the other hand, graphene-based materials are known for their chemical and mechanical stability, high surface area and relatively high capacitance values. Thus, it was logical combine the advantages of the excellent properties of both.

References:

1-Maxwell Ultracapacitors: Enabling Energy's Future. (n.d.). Retrieved from https://www.maxwell.com/products/ultracapacitors

2- Wang, G., Zhang, L., & Zhang, J. (2012). ChemInform Abstract: A Review of Electrode Materials for Electrochemical Supercapacitors. *ChemInform,43*(18). doi:10.1002/chin.201218217

3- *Kötz, R., & Carlen, M. (2000). Principles and applications of electrochemical capacitors. Electrochimica Acta,45(15-16), 2483-2498. doi:10.1016/s0013-4686(00)00354-6*

4- Winter, M., & Brodd, R. J. (2004). What Are Batteries, Fuel Cells, and Supercapacitors? *Chemical Reviews,104*(10), 4245-4270. doi:10.1021/cr020730k

5- Acharya, R., Subbaiah, T., Anand, S., & Das, R. (2002). Preparation, characterization and electrolytic behaviour of β-nickel hydroxide. *Journal of Power Sources,109*(2), 494-499. doi:10.1016/s0378-7753(02)00164-7

6- Kim, H., & Popov, B. N. (2003). Synthesis and Characterization of MnO -Based Mixed Oxides as Supercapacitors. *Journal of The Electrochemical Society,150*(3). doi:10.1149/1.1541675

7- Augustyn, V., Simon, P., & Dunn, B. (2014). Pseudocapacitive oxide materials for high-rate electrochemical energy storage. *Energy & Environmental Science,7*(5), 1597. doi:10.1039/c3ee44164d

8- Muzaffar, A., Ahamed, M. B., Deshmukh, K., & Thirumalai, J. (2019). A review on recent advances in hybrid supercapacitors: Design, fabrication and applications. *Renewable and Sustainable Energy Reviews,101*, 123-145. doi: 10.1016/j.rser.2018.10.026

Chapter 2: Theoretical background

2.1 Electrostatic capacitors Vs. supercapacitors

An electric capacitor has a sandwich structure comprising two conductive plates surrounding a dielectric or an insulator. Dielectrics include air, glass, or titanate. When an external voltage difference is applied across the two plates, a charging process takes place. During charging, the positive charges get accumulated on one plate (positive electrode) while the negative charges accumulate on the other plate (negative electrode). Removing the applied voltage leads both the positive and negative charges to remain at their corresponding electrodes, thus, separating electric charges. The difference in potential between the two electrodes is called the cell voltage. If the two electrodes are connected to a conductive wire coupled or not coupled with a load, a discharging process occurs, where the positive and negative charges gradually combine through this wire. In such way, the capacitor now can store and deliver energy. (1).

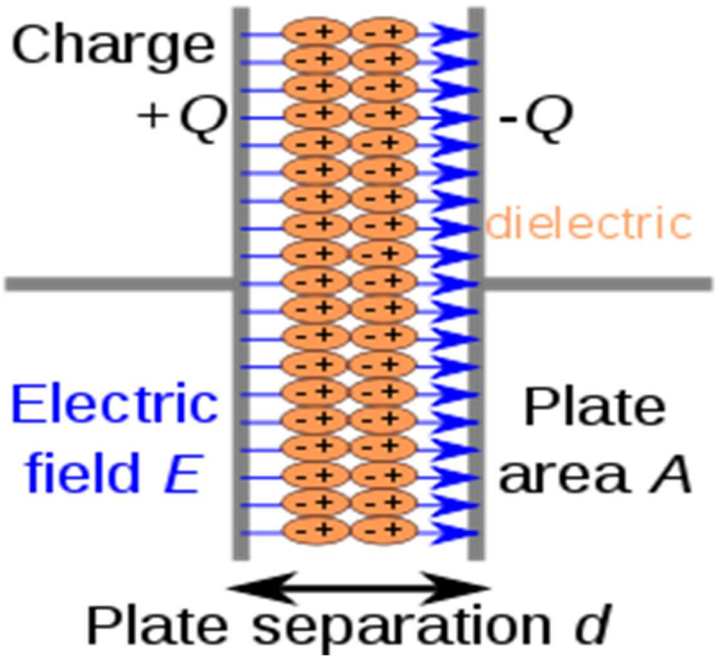

Fig.2.1: Schematic diagram of a charged capacitor (2)

Capacitance of an electrostatic capacitor (C) is related to the applied potential difference (V) and amount of charges stored(Q) by the following equation.

$$C = \frac{Q}{V} \qquad (2.1)$$

Energy stored in a capacitor related to its capacitance is given by:

$$w = \int_0^Q V dq = \int_0^Q \frac{q}{c} q dq = \frac{1}{2} c v^2 \qquad (2.2)$$

where V is the applied potential difference, Q is the amount of charges stored, and C is the capacitance. The maximum power of an electrostatic capacitor is:

$$P = \frac{W}{t} = \frac{1}{2} VI = \frac{1}{4} \frac{V^2}{R} \qquad (2.3)$$

where R is the series resistance.

The early idea of an electrochemical supercapacitor (ES) depended on the electric twofold layer existing at the interface between a conductor and the electrolyte. The electric double layer hypothesis was first proposed by Hermann von Helmholtz and further created by Gouy, Chapman, Grahame, and Stern. The electric twofold layer hypothesis is the establishment of electrochemistry from which the electrochemical procedures happening at an electrostatic interface between a charged electrode material and an electrolyte are researched. Considering this information, numerous electrochemical assumptions and advances including electrochemical supercapacitors, batteries have been created and built up since the double layer hypothesis was advanced. The first supercapacitor with high capacitance was invented by Becker at SOHIO in 1957.It operated in low voltage applications with carbon material as its electrodes. Fundamental understanding of the design, operation principle and materials used in supercapacitors led to development of such capacitors (increasing the energy density). To additionally increase energy density, further developed supercapacitors called pseudocapacitors, in which the electroactive materials are composited with carbon particles to frame composite electrode materials, were produced. (3,4).

2.2 Batteries, fuel cells, and supercapacitors.

2.2.1 Batteries versus fuel cells versus electrochemical supercapacitors

Electrochemical energy storage or conversion systems comprise batteries, fuel cells and supercapacitors. The electrochemical principles of the above mentioned three systems are the same, but restrictions on the electrons and ions conduction differ from one system to another. In case of batteries and power devices, electrical energy is produced due to redox reactions at the anode and cathode. In case of batteries anode and cathode act as the active mass, but in fuel cells anode and cathode are simply charge exchange media, and the dynamic mass admission originates from outside i.e. an oxygen tank for instance. As for electrochemical supercapacitors, energy is not necessarily transferred via redox reactions. By movement of electrolyte ions at the electrolyte/electrode interface, the so-called electrical double layers (EDLs) are evolved and, this results in a simultaneous flow of electrons in the external wire, and therefore energy is delivered (5).

2.2.2 Ragone plot

The terms energy density and power density can determine the performance of a fuel cell, battery, or a supercapacitor. Energy density ($\frac{w\,h}{L}$) is energy normalized per volume of electrode material. Specific power is a measure of how fast energy can be transferred.
Ragone plot is developed to compare power and energy density. Ragone plot shows that fuel cells possess the highest energy density among the three applications. Supercapacitors are characterized by the high-power density. Batteries are intermediate systems between supercapacitors and fuel cells, yet batteries possess higher energy density than that of supercapacitors.

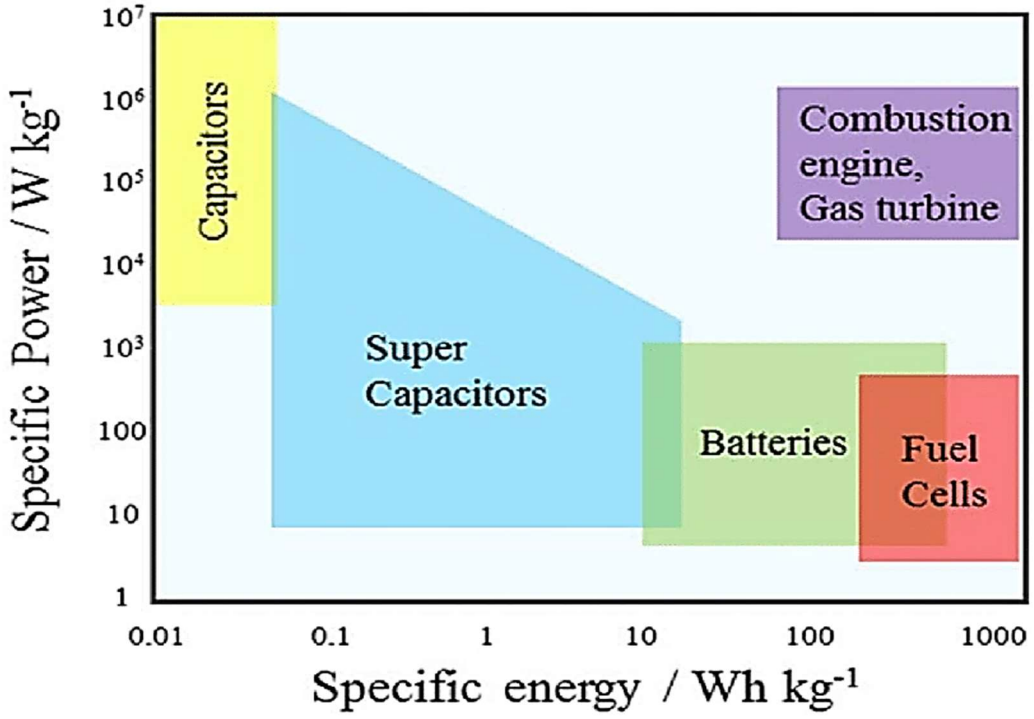

Fig.2.2: Ragone plot (6)

2.2.3. Kinetics of an electrochemical system

The difference between thermodynamics and kinetics is that thermodynamics determines whether a reaction can occur, energy associated (released or gained) during a reaction. On the other hand, kinetics determines the rate at which a reaction occurs. kinetics of a process is generally about how to overcome the energy barrier to finish the transformation from the starting (reactant) state to the final (product) state. Another key difference between them is that thermodynamics is concerned with systems in stable or metastable states, while kinetics is applicable to systems in transition from nonequilibrium to equilibrium, or between two equilibrium states. (11).

Kinetics of electrodes and chemical kinetics are different from each in two aspects: (1) the potential drop at the electrode / electrolyte interface, and (2) The 2D reactions that take place at the electrode / electrolyte interface. In any electrochemical reaction, charge transfer process takes place, where kinetics of polarization effect must be considered. Polarization effects can be classified into three main categories; activation polarization, concentration polarization and ohmic polarization. (7).

Activation potential refers to the over potential caused by the rate determining step of the reaction, in such case it is the energy needed for a charge transfer reaction to proceed. The rate determining step of a reaction is due to dissociation of the activated complex, i.e. activation energy of the redox reaction, the rate, current flow, of a charge-transfer-controlled battery reaction can be given by the Butler-Volmer equation as:

$$i = i_{\circ} \exp[\frac{\alpha F\eta}{RT} - \frac{(1-\alpha)F\eta}{RT}] \qquad (2.4)$$

where i is the normalized current flow (I/A). A is the electrode surface area. $i_{\circ}$ is the exchange current density $i_{\circ}=k_{\circ}FA$ (A here being the activity product, K is the reaction rate constant), α is the transfer coefficient, η is the polarization ($\eta=E-E_{\circ}$) (7,12). Another type of polarization occurs as a result of variation of the active species from the surface of an electrode/electrolyte to the bulk. Such polarization is named “concentration polarization”. It is a result of the limited mass transport capabilities. Concentration polarization is given by:

$$\eta = \ln \frac{RT}{n} \frac{c}{c_{\circ}} \qquad (2.5)$$

C and $C_{\circ}$ are the concentration of material at the electrode interface and in the bulk of the electrode/electrolyte. (13).

Ohmic polarization evolves as a result of the configuration of the electrochemical cell itself. It is due to ionic resistance of the electrolyte, resistance between current collector and the electrode material , and diffusion of ions of the ectrolyte. Such ohmic polarization leads to what so-called “IR drop”. Ohmic polarization is given by:

$$\eta=IR \qquad (2.6)$$

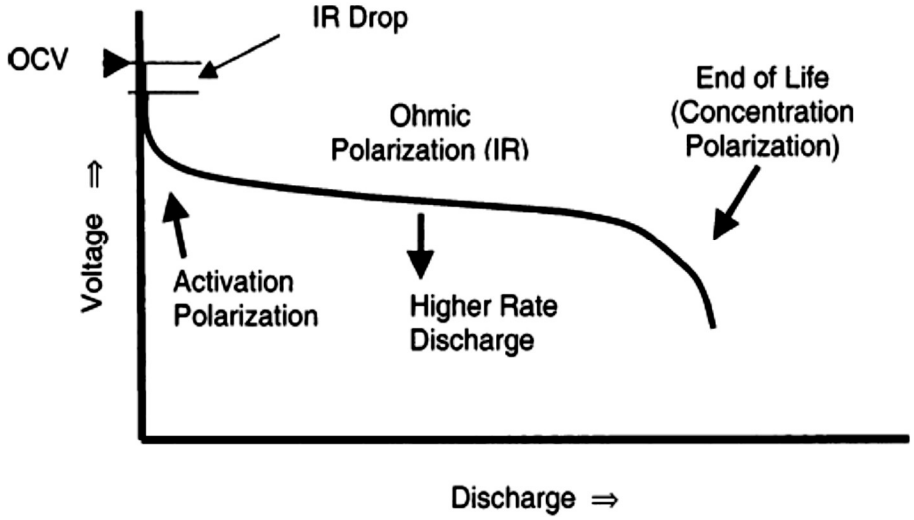

Fig.2.3: Schematic diagram of a discharge curve of a battery. (5).

2.3 Classification of supercapacitors

Supercapacitors are classified according to charge separation mechanism into double layer, pseudocapacitors and hybrid capacitors.

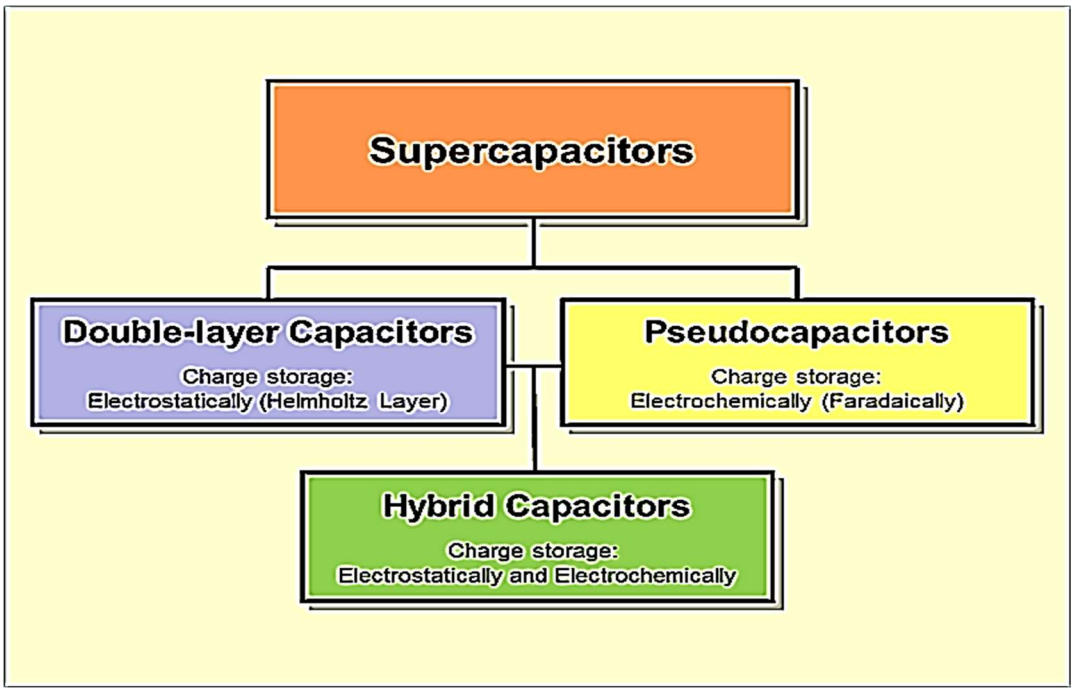

Fig.2.4: Classification of supercapacitors (2)

2.3.1 Electrochemical double-layer supercapacitors

Supercapacitors are electrochemical double layer energy storage devices. The concept of a supercapacitor is based on the electrical double layer existing at the interface between an electrode and its conducting electrolytic solution. Electrochemical supercapacitors are made of two electrodes separated by an electrolytic solution. The electrolytic solution between the two electrodes can either be a liquid or solid state. In addition to being physical separators between the two electrodes, Solid state electrolytes act as ionic conductors. Figure 5.2 shows a typical double-layer capacitor. The whole charge transfer mechanism is non-faradic, where, on the cathode, a gathering of positive charges pulls in an equivalent number of negative charges around the electrode in the electrolyte side because of Coulomb's force, but because of heat fluctuation in the electrolyte; the charges carried by the particles have a scattered distribution, prompting some net negative charges in the electrolyte zone close to the cathode. This charge adjustment between the electrode and the electrolyte represents an electric double layer. To keep up the electric neutrality of bias of the framework, an equivalent number of negative charges collect at the negative anode, where an equivalent number of net positive charges in the neighboring electrolyte, shaping another twofold layer. Subsequently, an entire double layer capacitor has two electric double layers, one at the positive electrode/electrolyte interface and the other at the negative electrode– electrolyte interface. These two twofold layers constitute the capacitor's "heart" and decide its performance. (14,15).

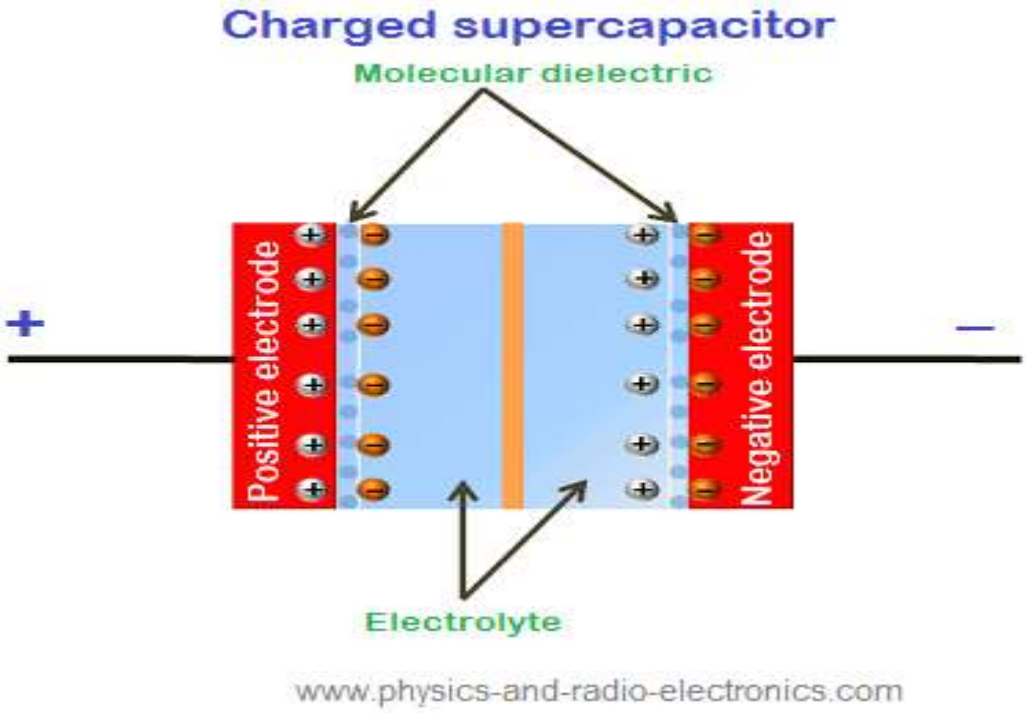

Fig.2.5: Electric double-layer supercapacitor (48).

2.3.1.1 Diffuse layer

As discussed before, the electric double layer is formed due to accumulation of positive ions near the anode, and negative ions near the cathode side. However, due to heat fluctuation, ions may get scattered with a higher concentration near the electrode-electrolyte interface, and a lower concentration within the solution. This scattered layer in addition to the positive or negative charge array is named , the Gouy-Chapmen diffuse layer or simply diffuse layer. (16). The thickness of this diffuse layer is a function of temperature, electrolyte concentration, and its dielectric constant, and the charge number carried by the ions. At lower temperature, higher concentration of electrolytic solution, charge number and dielectric constant of the electrolyte, diffuse layer gets very compact and thinner. This compact layer is called the Helmholtz layer, which is divided into inner and outer plane. (17). The Helmholtz layer in addition to the Gouy- chapmen charge distribution model illustrates the double layer interface model (Stern-Grahame model) (17).

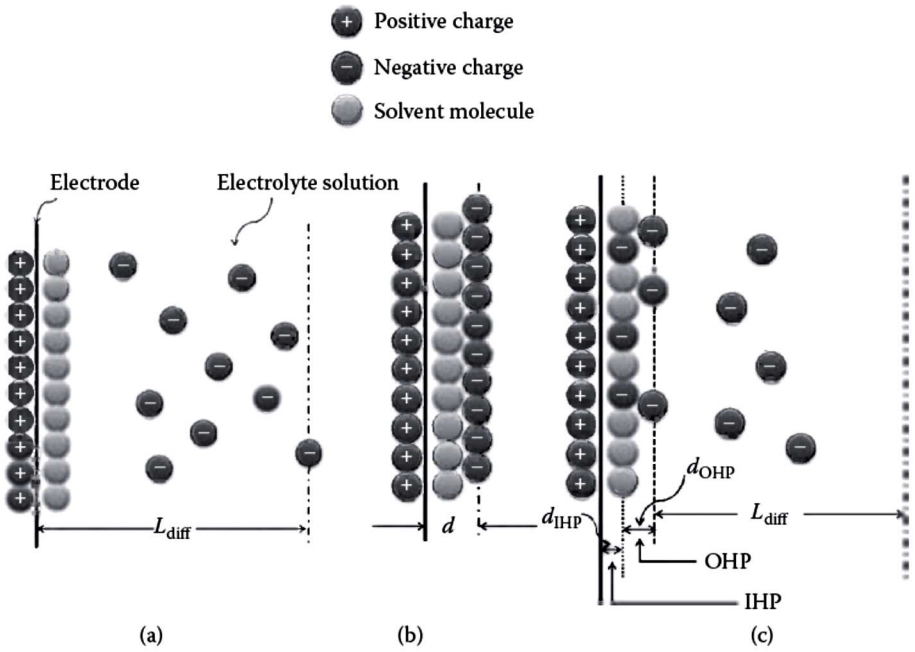

Fig.2.6: Double-layer models at interface of electrode and electrolyte solution. (a) Diffuse layer or Gouy-Chapman model. (b) Helmholtz layer or model; the *d* represents the double-layer thickness. (c) Stern-Grahame layer or model in which the IHP represents the inner Helmholtz plane and the OHP is the outer Helmholtz plane. (49).

2.4 Calculations of EDL

2.4.1 Specific capacitance

Specific capacitance is the key factor of determining a supercapacitor's performance. Specific capacitance is defined as the total capacitance of the two-electric double-layers divided by the electrode's surface area. (20).

$$csp = \frac{c}{m} \qquad (2.7)$$

where c is the total capacitance of the electric double-layers, and m is the mass of the active electrode's material.

2.4.2 Energy density

Energy density of a supercapacitor is one of the crucial factors that determine its performance. In a double layer supercapacitor energy density is expressed as:

$$E = \int_0^q V dq = \int_0^q \frac{q}{c} dq = \frac{\frac{1}{2}q^2}{c} = \frac{1}{2}CV^2 \qquad (2.8)$$

In practical applications, the specific energy density is more widely used.

$$E = \frac{1}{2}Csp\ V^2 \qquad (2.9)$$

Energy density is dependent on materials used. A stable material with higher voltage window leads to increasing the power density. Also, diverse current collectors' materials have distinctive densities. Lighter, highly conductive, and more stable current gatherer materials are constantly needed. Besides, the interaction of the electrolyte ions and the electrode's layer can likewise assume a part in changing the energy density of a supercapacitor by adjusting the differential capacitance. (21).

2.4.3 ESR (equivalent series resistance)

If a sinusoidal elective current is applied on a perfect capacitor, the yield voltage is ought to be out of phase by 90°. In a supercapacitor, the output voltage is ordinarily out of stage less than 90°, recommending that an equivalent series resistor coupled. Such ohmic component is the equivalent series resistance (ESR). This series resistance includes: the contact resistance between the present current collector and the electrode layer, the ionic *(diffusion)* resistance of ions moving in small pores**,** and electrolyte ionic resistance. (22).

2.4.4 Power density

Power density determines the rate at which energy is transmitted to an external load. The definition of power density is the cell voltage multiplied by its current density. (23)

$$P = \frac{I}{m} vcell \qquad (2.10)$$

The discharge current (I) can cause the reduction of initial voltage (V_i) to the real time Voltage $V=V_i-IR_s$. The corresponding power $P=VI=V_iI-I_2R_s$. To reach the maximum power, $dP/dI=0$. So $I_{Pmax}=V_i/2R_s$ and $V_{Pmax}=V_i-IR_s=V_i/2$. Then the P_{max} has the formula.

$$P = \frac{1}{4m}\frac{V^2}{R} \qquad (2.11)$$

2.5 Pseudocapacitors

The idea of supercapacitors evolved to modify the properties of ES and increase its capacitance value. ES have relatively small values of specific capacitance as it depends only on the electrode's surface area, such as carbon. Besides, the ion electrolyte accessibility of the carbon porous structure is low. In order to increase the capacitance of ES, electrochemically active materials are introduced as anode and cathode materials. Those electrochemically active materials provide higher pseudo capacitance than the active materials of the Double layer supercapacitors. Pseudo capacitance charge storage mechanism on a very basic level differs from that of Electrochemical double layers. In case of pseudocapacitors charge transfer is through a thermodynamically and kinetically favoured faradic (electrochemical) reaction. In practical applications, the electrode layer of a pseudocapacitors consists of both electrochemical materials such as carbon-based materials, and a solid- state redox material that contributes to pseudo capacitance. In such case the charge transfer mechanism involves both faradic and non-faradic reactions. (24).

For electrochemical redox reactions (oxidation and reduction), each reactant molecule in the bulk phase donates one or more charges toward the stored energy, unlike the case in a double-layer charging or discharging process where only charges can physically adsorb on the material particle's surface. Therefore, pseudo capacitance is much higher than that of the double layer capacitance. (25). Materials used in pseudocapacitors must be

electrochemically reversible. Electrochemical reversibility means that both oxidation and reduction process occur at the same electrode potential. However, in practice redox reactions are not very reversible, and limited by reaction kinetics. (50).

2.5.1 Basic electrochemistry of pseudocapacitors

Thermodynamics assumes a comparative part in physical chemistry like arithmetic in mathematics, but the relationship between thermodynamics and electrochemistry is not that clear. (5). An important term to start with would be the definition of an electrode. An electrode comprises of two or more electrically conducting states connected in series, where charge carriers (ions or electrons) can be exchanged, one of the terminal phases is an electron conductor and the other being an electrolyte. The electronic conductor can be an alloy, metal oxide, a semi-conductor, …etc. The electrode taking place in oxidation process is the anode. On the other hand, the electrode responsible for reduction is the cathode. (7), (8). Another important definition is the "electrode potential". It can be defined as the potential difference between a certain electrode and the reference electrode. (8).The basic thermodynamic equation describing a reversible electrochemical transformed system is Gibb's free energy equation given by:

$$\Delta G = \Delta H - T\Delta S \qquad (2.12)$$

where ΔG is the Gibb's free energy. It represents amount of free energy available for a reaction to occur. ΔH is the energy released off a system (Enthalpy). TΔS represents the heat associated due to disorder in the system. It should be noted that ΔG ,ΔH and ΔS are state functions which depend only on the initial and final states of the reaction. In an electrical point of view, Gibb's free energy is given by

$$\Delta G = -nFE \qquad (2.13)$$

F is faraday's constant, E is the electromotive force of the cell, and n is the number of electrons involved in the electrochemical reaction. This equation represents the net available electrical energy from a reaction. The quantity (nF) is the amount of electricity produced and is proportional to the amount of material used. For bulk chemical reaction Van't Hoff isotherm comes into play.

$$\Delta G = \Delta G^{\circ} + RT \ln(\frac{Ap}{Ar}) \qquad (2.14)$$

where R is the universal gas constant, T is the absolute temperature, Ar and Ap are the activity product of products and reactants. Nernest equation is another crucial equation to consider since it determines the potential of an electrochemical system at nonstandard conditions. Nernest equation is given by:

$$E = E^{\circ} + \frac{RT}{nF}\ln(\frac{Ap}{Ar}) \qquad (2.15)$$

Faraday's laws, as given in equation 2.16,illustrates the relationship between current flow and amount of material. (5, 9, 10).

$$g = \frac{It(MW)}{nF} \qquad (2.16)$$

2.6 Hybrid supercapacitor

In a hybrid supercapacitor system, both carbon-based materials and electrochemically active (redox materials) are used simultaneously to make use of the merits of ES and pseudocapacitors and enhance their drawbacks. In such case, both faradic and non-faradic (electrostatic) charge storage mechanisms are incorporated. Both double-layer capacitance and pseudo capacitance can be achieved in single ES device to form a hybrid system. Because both Faradaic process and non-Faradaic process are used, high performance electrode materials, and better energy and power performance is achievable, with high class performing supercapacitor. Hybrid systems are themselves classified into three main categories, asymmetric supercapacitor, symmetric supercapacitor and battery-like supercapacitor. (26).

2.6.1 Asymmetric hybrid supercapacitors

Asymmetric hybrid supercapacitors consist of two different electrodes, with one of a carbon-based material (double layer capacitance), and the other one of a redox material (pseudo capacitance dominates). Such system is characterized by the high cycling stability when compared to pseudocapacitors. (27).

2.6.2 Symmetric hybrid supercapacitors

Symmetric supercapacitors are made of two similar electrodes, with redox species anchored on the carbon – based material surface. This leads to improving the device's electrochemical properties and enhancing the overall performance. Also, composite electrodes (made of carbon-based materials and redox species) acting as the two electrodes, can be regarded as symmetric hybrid supercapacitors (28).

2.6.3 Battery-like supercapacitors

In such configuration, a battery-like material is use such as Li, and a carbon–based electrode is the other one. Such devices makes use of the high energy density property of batteries, and the EDL material's' high-power density (29)

2.7Applications of supercapacitors

Applications of ES include consumer electronics. Supercapacitors are widely used in consumer electronics as back-up energy sources for system memories, microcomputers, and so on. They are very practical because of their long-life cycles when compared to batteries. Other applications include transportation. In such application, supercapacitors are couples with fuel cells. Supercapacitors provide sudden bursts of energy when starting up, and fuel cells on the other hand provide sustained energy. Other applications include, smart grids, smart cloth and cell phone towers. (30).

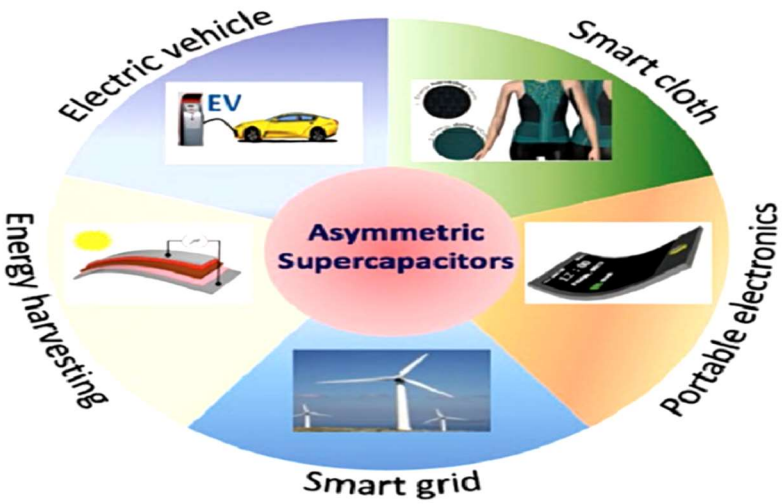

Fig.2.7: Applications of Supercapacitors (30)

2.8 Components for supercapacitors

Optimizing the design and operation of ES includes fine selection of electrode materials, separators, electrolytic solutions, sealants and current collectors. Electrode materials are ought to be highly conductive, highly porous and of high BET surface area. Current collectors must also be highly conductive to enable electron transfer through an external circuit. Electrolytes criteria of choice are the high mobility of ions, low toxicity, wide range of operating voltage (wide voltage window) and safety. As for the sealants, they are chosen to be porous, that is to allow ions transfer from the electrolyte to the electrode surface. In addition to this, they must be electronically insulating to avoid short circuiting. (31). Detailed considerations of the components used in supercapacitors will be discussed in below.

2.8.1 Electrode requirements for supercapacitors

Requirements for optimizing the electrode materials are the following:

- High conductivity
- Chemical stability over a wide range of operating voltage.
- The voltage window of the electrolyte.
- High specific surface area
- Excellent mechanical stability.

2.8.1.1 Electrical conductivity of the electrode material

Great electrical conductivity is imperative in empowering ES devices to work at high power. Upon discharge, charges stored inside the material should successfully move through the thick anode layers and out to the circuit. Electron transport is reliant upon the nature of conductive pathways inside the material and the conductivity of the material utilized as a part of the cathode. On the off chance that the conduction through the cathode isn't sufficiently enough or the way is excessively convoluted. (32).

2.8.1.2 High specific surface area

High electrode's surface area contributes in enhancing the performance of the ES device. This allows more ions from the electrolyte to be arranged at the electrode's surface. It is better to have a porous electrode material to increase the accessibility of ions. Maximizing the specific surface area leads to increasing the number active sites allowed for ions, and thus improving the properties of the supercapacitor. However, it should be noted that pore size has to be reasonable (mesoporous‹50 nm) to avoid having blocked pores or tightly bound planes that prevent ions from ordering at the surface of the electrode. (33), (34).

Relation between pore radius size b, capacitance C and surface area of the electrode A is given as follows:

$$\frac{C}{A} = \frac{\varepsilon_{\circ}\varepsilon r}{b ln\left(\frac{b}{a_{\circ}}\right)} \qquad (2.17)$$

$\varepsilon_{\circ}$and εr are the permittivity of vacuum and electrolyte, and $a_{\circ}$ is the effective size of the ion. (35).

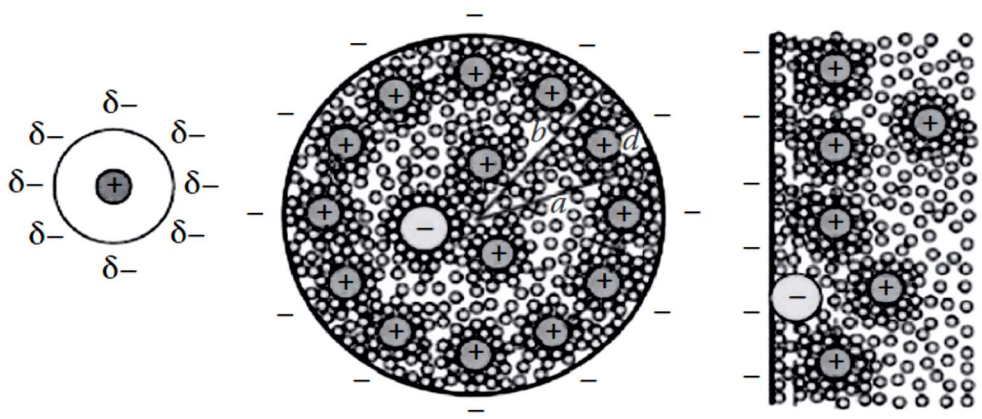

Fig 2.8: Effect of pore size on supercapacitor ‘s specific surface area (49).

2.8.2 Current collectors

Current collectors in ES are used to gather the electrical charges (electrons) stored in the electrode's active material. Usually, conduction of charges supplied by the electrode's active material is insufficient and leads to series resistance. For this reason, material of choice of the current collectors are metals such as aluminum, copper, etc. Unfortunately, with time the connection between the current collector and the electrode material can degrade due to the loss of the actual electrode material. These losses lead to shrinkage in the overall performance of the ES. Such affected properties are the life cycle and the overall capacitance. The direct contact between the electrode and the current collector leads to high series resistance. To avoid the drawbacks of this undesirable series resistance is increasing the surface roughness of the active material by plating it with either silver, gold or lead. (36), (37).

2.8.3 Separators

Separators are designed to prevent the contact between the two electrodes (cathode and anode). Separators should be mechanically strong and ionic conductive. They also should prevent migration of the actual active species of the materials used. Separators materials are mica, glass, ceramic and paper-based separators. (38).

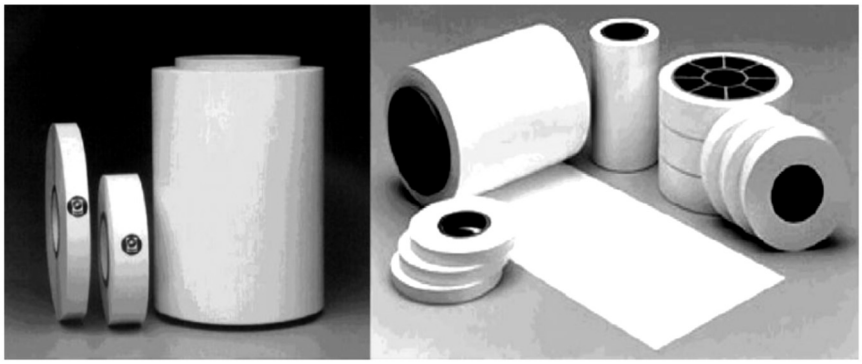

Fig. 2.9: Ceramic-based separators (38)

2.8.4 Electrolytes

Electrolytic solutions play an essential role in improving the performance of a supercapacitor. Electrolytes are ought to be of high ionic conductivity, reasonable ionic size, good chemical and mechanical stability, high operating temperatures, large potential windows, low corrosion potential and low flammability. The above-mentioned factors in addition to the electrolyte-electrode interactions must be considered in order to avoid break down of materials, increased series resistance and the life cycle durability of an ES. Electrolytes are classified into several main categories such as ionic electrolytes, organic, solid-state and aqueous electrolytes. (39).

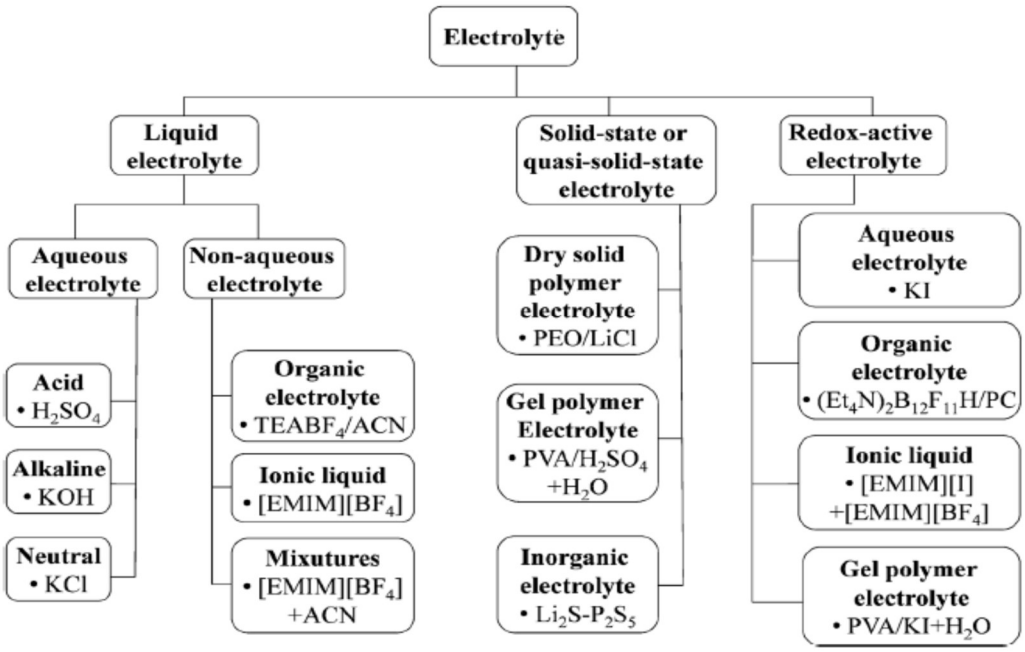

Fig.2.10: Classification of electrolytes reference (39)

2.8.4.1 Aqueous electrolytes

Aqueous electrolytes are grouped into alkaline, acidic and neutral solutions, such as Potassium hydroxide, sulphuric acid and sodium sulphide. In general, aqueous electrolytes are characterized by their high ionic conductivity, mobility, and the contribution to higher specific capacitance values. On the other hand, aqueous electrolytes have some disadvantages such as, corrosion, reduced life cycle and low voltage window. Such low

voltage stability poorly restricts the performance of an ES such as the energy and power density values. (40).

Table (2.1) electrolyte resistance and voltage of various aqueous electrolytes (42).

Electrolyte Solution	Density (g/cm^3)	Conductivity (mS/cm)	ΔU
Aqueous, KOH	1.29	540	1
Aqueous, KCl	1.09	210	1
Aqueous, sulfuric acid	1.2	750	1
Aqueous, sodium sulfate	1.13	91.1	1
Aqueous, potassium sulfate	1.08	88.6	1
Propylene carbonate, Et_4NBF_4	1.2	14.5	2.5 to 3
Acetonitrile, Et_4NBF_4	0.78	59.9	2.5 to 3
IL, $Et_2MeIm^+ BF_4$	1.3 to 1.5	8 (25°C)	4
IL, $Et_2MeIm^+ BF_4$		14 (100°C)	3.25

2.8.4.2 Organic electrolytes

Organic electrolytes are commonly used due to their wide potential window in the range of 2.5 V to 2.8 V. This wide potential window leads to higher power and energy density values. Organic electrolytic solutions used include conductive salts such as Acetonitrile. However, there are some issues concerning organic electrolytes. Those concerns are the toxicity of the organic material, flammability and the small specific capacitance values. (43).

In EDLCS organic electrolytes lead to lower specific capacitance values than aqueous electrolytes because organic electrolytes have large solvated ion size and low dielectric constants. In EDLCS, specific capacitance depends on the pore size distribution of carbon -based materials. Carbon materials with small pore size are not favorable because they limit the accessibility of the electrolyte's ions. Therefore, its essential to match the size of the pores in the carbon-based material and the electrolyte's ion size to increase the values of the specific capacitance. (44).

Table (2.2) relation between pore size, capacitance and internal resistance. (45)

Capacitor	Negative Electrode	Positive Electrode	Volumetric Capacity (F/cm^3)	Internal Resistance (mΩ)
1	A	B	26.6	24
2	A	A	20.8	23
3	B	B	27.5	257
4	B	A	18.8	243

2.8.4.3 Ionic liquids

Ionic liquids consist of molten salts made entirely of ions. They are characterized by the low melting point, high chemical stability, wide potential window, low toxicity and high chemical stability. However, they suffer from the low ionic conductivity, and high heat outcome. (46).

2.8.4.4 Solid state polymer electrolytes

Gel and solid-state polymer electrolytes are meant to combine functions of both the electrolyte and the separator in an ES. Examples include PVA and PVDF. Solid state and gel electrolytes are characterized by the high stability, ion conductivity and wide potential window. Yet, penetration of ions is a major drawback because of the electrolyte's thickness. (47).

References:

1-Size, S. M. (2006). *Physics of Semiconductor Devices, 3rd Edition* (3rd ed.).

2-Capacitor. (2019, March 12). Retrieved from https://en.wikipedia.org/wiki/Capacitor

3- Kötz, R., & Carlen, M. (2000). Principles and applications of electrochemical capacitors. *ElectrochimicaActa,45*(15-16),2483-2498.doi:10.1016/s0013-4686(00)00354-6

4- Zhang, L. L., & Zhao, X. S. (2009). ChemInform Abstract: Carbon-Based Materials as Supercapacitor Electrodes. *ChemInform,40*(47). doi:10.1002/chin.200947213

5- Winter, M., & Brodd, R. J. (2004). What Are Batteries, Fuel Cells, and Supercapacitors? *ChemInform,35*(50). doi:10.1002/chin.200450265

6- Taberner, P., Heitbaum, J., & Vielstich, W. (1976). The influence of the electrolyte composition on the formate oxidation in alkaline formate-air fuel cells. *Electrochimica Acta,21*(6), 439-440. doi:10.1016/0013-4686(76)85122-5

7- Inzelt, G. (2014). Crossing the bridge between thermodynamics and electrochemistry. From the potential of the cell reaction to the electrode potential. *ChemTexts,1*(1). doi:10.1007/s40828-014-0002-9

8- Inzelt, G. (2013). *Handbook of Reference Electrodes*. Springer.

9- Parsons, R. (1974). Electrochemical nomenclature. *Pure and Applied Chemistry,37*(4), 499-516. doi:10.1351/pac197437040499

10- Bard, A. J. (2008). *Electrochemical Dictionary*. Springer.

11- Admin, & About the Author: Adm incoming from Engineering cum Human Resource Development background. (2012, May 17). Thermodynamics vs Kinetics. Retrieved from https://www.differencebetween.com/difference-between-thermodynamics-and-vs-kinetics/

12- Soestbergen, M. V. (2012, June 10). Frumkin-Butler-Volmer theory and mass transfer inelectrochemicalcells.Retrievedfromhttps://link.springer.com/article/10.1134/S10231935

12060110

13- Bonnefont, A. (2001). *Electroanalytical Chemistry,500*, 52-61.

14- Stern, O. (1924). The theory of electrolytic double shift. *Elektrochemie Und Angewandte Physikalische Chemie Banner.,30*, 508-516.

15- Burke, A. (2007). R&D considerations for the performance and application of electrochemical capacitors. *Electrochimica Acta,53*(3), 1083-1091. doi: 10.1016/j.electacta.2007.01.011

16- Grahame, D. C. (1947). The Electrical Double Layer and the Theory of Electrocapillarity. *Chemical Reviews,41*(3), 441-501. doi:10.1021/cr60130a002

17- Soffer, A., & Folman, M. (1972). The electrical double layer of high surface porous carbon electrode. *Journal of Electroanalytical Chemistry and Interfacial Electrochemistry,38*(1), 25-43. doi:10.1016/s0022-0728(72)80087-1

18- Stern, O. (1924). The theory of electrolytic double shift. *Elektrochemie Und Angewandte Physikalische Chemie Banner.,30*, 508-516.

19- Rankin, D. W. (2009). CRC handbook of chemistry and physics, 89th edition, edited by David R.Lide. *CrystallographyReviews,15*(3),223-22doi:10.1080/08893110902764125

20- Black, J., & Andreas, H. A. (2009). Effects of charge redistribution on self-discharge ofelectrochemicalcapacitors. *ElectrochimicaActa,54*(13),35683574.doi:10.1016/j.electact a.2009.01.019

21- Oickle, A. M., & Andreas, H. A. (2011). Examination of Water Electrolysis and Oxygen Reduction as Self-Discharge Mechanisms for Carbon-Based, Aqueous Electrolyte Electrochemical Capacitors. *The Journal of Physical Chemistry C,115*(10), 4283-4288. doi:10.1021/jp1067439

22- Portet, C., Yang, Z., Korenblit, Y., Gogotsi, Y., Mokaya, R., & Yushin, G. (2009). Electrical Double-Layer Capacitance of Zeolite-Templated Carbon in Organic Electrolyte. *Journal of The Electrochemical Society,156*(1). doi:10.1149/1.3002375

23- Portet, C., Taberna, P., Simon, P., & Laberty-Robert, C. (2004). Modification of Al current collector surface by sol–gel deposit for carbon–carbon supercapacitor applications. *Electrochimica Acta,49*(6), 905-912. doi: 10.1016/j.electacta.2003.09.043

24- Bard, A. J. and L. R. Faulkner. 1980. *Electrochemical Methods, Fundamentals, and Applications,* New York: John Wiley & Sons.

25- Grigorchuk, I. I. 2003. Redox processes and pseudocapacitance of capacitors in light of intercalation. Nanotechnologies, 39, 770–773.

26- Zhao, J. H., Michalski, W. P., Williams, C., Li, L., Xu, H., Lamb, P. R., . . . Dai, X. J. (2011). Controlling cell growth on titanium by surface functionalization of heptylamine using a novel combined plasma polymerization mode. *Journal of Biomedical Materials Research Part A,97A* (2), 127-134. doi:10.1002/jbm.a.33035

27- Wang, H., Liang, Y., Mirfakhrai, T., Chen, Z., Casalongue, H. S., & Dai, H. (2011). Advanced asymmetrical supercapacitors based on graphene hybrid materials. *Nano Research,4*(8), 729-736. doi:10.1007/s12274-011-0129-6

28- Dubal, D. P., Suarez-Guevara, J., Tonti, D., Enciso, E., & Gomez-Romero, P. (2015). A high voltage solid state symmetric supercapacitor based on graphene–polyoxometalate hybrid electrodes with a hydroquinone doped hybrid gel-electrolyte. *Journal of Materials Chemistry A,3*(46), 23483-23492. doi:10.1039/c5ta05660h

29-Yu, S., Yang, N., Zhuang, H., Mandal, S., Williams, O. A., Yang, B., . . . Jiang, X. (2017). Battery-like supercapacitors from diamond networks and water-soluble redox electrolytes. *Journal of Materials Chemistry A,5*(4), 1778-1785. doi:10.1039/c6ta08607a

30- Roldán, S., Barreda, D., Granda, M., Menéndez, R., Santamaría, R., & Blanco, C. (2015). An approach to classification and capacitance expressions in electrochemical capacitors technology. *Physical Chemistry Chemical Physics,17*(2), 1084-1092. doi:10.1039/c4cp05124f

31-Simon, P., & Gogotsi, Y. (2008). Materials for electrochemical capacitors. *Nature Materials,7*(11), 845-854. doi:10.1038/nmat2297

32- Qu, D., & Shi, H. (1998). Studies of activated carbons used in double-layer capacitors. *Journal of Power Sources,74*(1), 99-107. doi:10.1016/s0378-7753(98)00038-x

33- Huang, J., Sumpter, B., & Meunier, V. (2008). A Universal Model for Nanoporous Carbon Supercapacitors Applicable to Diverse Pore Regimes, Carbon Materials, and Electrolytes. *Chemistry-AEuropeanJournal,14*(22),6614-6626. doi:10.1002/chem.200800639

34- Chmiola, J. et al. 2006. Anomalous increase in carbon capacitance at pore sizes less than 1 nanometer. *Science*, 313, 1760–1763

35- Feng, G., Qiao, R., Huang, J., Sumpter, B. G., & Meunier, V. (2010). Atomistic Insight on the Charging Energetics in Subnanometer Pore Supercapacitors. *The Journal of Physical Chemistry C,114*(41), 18012-18016. doi:10.1021/jp107125m

36- Wu, H., Lin, Y., Lee, E., Lin, W., Hu, J., Chen, H., & Wu, N. (2009). High-performance carbon-based supercapacitors using Al current-collector with conformal carbon coating. *Materials Chemistry and Physics,117*(1), 294-300. doi: 10.1016/j.matchemphys.2009.06.001

37- Portet, C., Taberna, P., Simon, P., & Laberty-Robert, C. (2004). Modification of Al current collector surface by sol–gel deposit for carbon–carbon supercapacitor applications. *Electrochimica Acta,49*(6), 905-912. doi: 10.1016/j.electacta.2003.09.043

38- Arora, P., & Zhang, Z. (. (2004). Battery Separators. *Chemical Reviews,104*(10), 4419-4462. doi:10.1021/cr020738u

39- Zhong, C., Deng, Y., Hu, W., Qiao, J., Zhang, L., & Zhang, J. (2015). A review of electrolyte materials and compositions for electrochemical supercapacitors. *Chemical Society Reviews,44*(21), 7484-7539. doi:10.1039/c5cs00303b

40- G. P. Xiong, C. Z. Meng, R. G. Reifenberger, P. P. Irazoqui and T. S. Fisher, Electroanalysis, 2014, 26, 30–51.

41-19- Rankin, D. W. (2009). CRC handbook of chemistry and physics, 89th edition, edited by David R. Lide. *Crystallography Reviews,15*(3), 800-900. doi:10.1080/08893110902764125

42- Burke, A. (2007). R&D considerations for the performance and application of electrochemical capacitors. *Electrochimica Acta,53*(3), 1083-1091. doi: 10.1016/j.electacta.2007.01.011

43- Tiruye, G. A., Muñoz-Torrero, D., Berthold, T., Palma, J., Antonietti, M., Fechler, N., & Marcilla, R. (2017). Functional porous carbon nanospheres from sustainable precursors for high performance supercapacitors. *Journal of Materials Chemistry A,5*(31), 16263-16272. doi:10.1039/c7ta01951c

44*McDonough*, *J.K.*, *Frolov*, *A.I.*, *Presser*, *V.*, *Niu*, *J.*, *Miller*, *C.H.*, *Ubieto*, *T.*, *Fedorov*, *M.V.*, and *Gogotsi*, *Y.* (*2012*) Influence of the structure of *carbon* onions on their electrochemical performance in supercapacitor electrodes. ... *Carbon*, *50* (9), *3298–3309*

45- Yu, A., Chabot, V., & Zhang, J. (2017). Electrochemical Supercapacitors for Energy Storage and Delivery. doi:10.1201/b14671

46- Lewandowski, A., Olejniczak, A., Galinski, M., & Stepniak, I. (2010). Performance of carbon–carbon supercapacitors based on organic, aqueous and ionic liquid electrolytes. *Journal of Power Sources,195*(17), 5814-5819. doi: 10.1016/j.jpowsour.2010.03.082

47- Lian, K., & Li, C. M. (2009). Solid polymer electrochemical capacitors using heteropoly acid electrolytes. *Electrochemistry Communications,11*(1), 22-24. doi: 10.1016/j.elecom.2008.10.016

48-Shaik, A. (n.d.). Retrieved from https://www.physics-and-radio-electronics.com/electronic-devices-and-circuits/passive-components/capacitors/supercapacitor.html .

49- Lu, M. (2013). *Supercapacitors: Materials, Systems, and Applications*. Weinheim: Wiley.

50- Mao, J., Iocozzia, J., Huang, J., Meng, K., Lai, Y., & Lin, Z. (2018). Graphene aerogels for efficient energy storage and conversion. *Energy & Environmental Science,11*(4), 772-799. doi:10.1039/c7ee03031b

Chapter Three

Literature survey

3.1 Introduction

This section offers a brief review on the different graphene-based electrode materials used in supercapacitors, methods of preparation of Graphene as well as reduction mechanisms and approaches.

3.1.1 Graphite and Graphene.

Graphite is a carbon allotrope which is multilayers of graphene. It is made of sp2 hybridized carbon atoms. Graphite is electrically conductor, making it a perfect candidate for electro-chemical applications. (1), (3). But Graphite cannot be used as a structural material alone due to its sheer planes. (4).

Graphene is the monolayer sheets of Graphite that are stacked in a hexagonal structured lattice. Graphene is an excellent promising material due to its high electronic conductivity, mechanical strength, and high surface area. Graphene is considered the building block of all graphitic-based materials.(4,5) mentioned, Graphite cannot be employed as a structural material on its own. It is graphene, graphene oxide (GO) or Reduced graphene oxide (rGO) that can be employed.

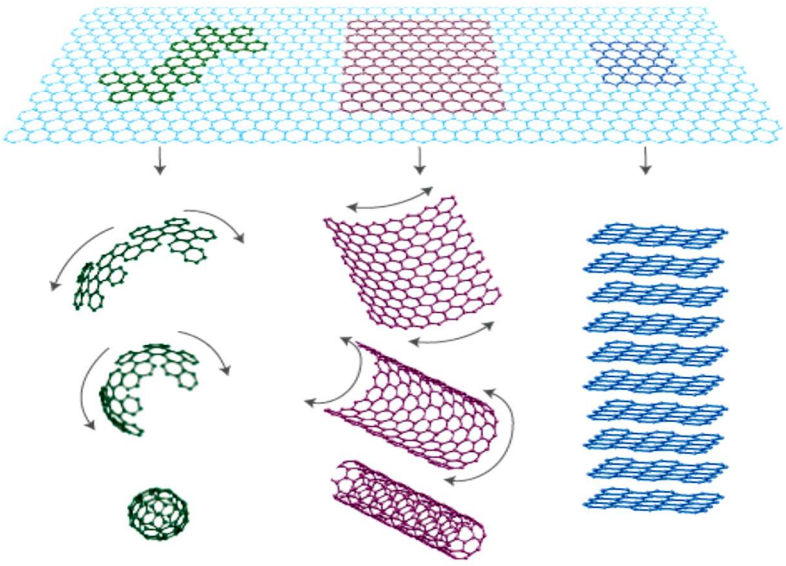

Fig 3.1: 0D Bucky balls, 1D nanotubes and 3D graphene (4).

3.2 Preparation of Graphene

Bottom up approaches

3.2.1 Chemical vapour deposition approach

Chemical vapour deposition (CVD) can be defined as the process of depositing gaseous reactants into a substrate. This reaction takes place in a confined reaction chamber, where temperature, pressure and precursor gases are scalable and pre-set. In general, in a CVD reactor, a thin substrate is used on which the target material film is grown. One of the main advantages of growing thin film using CVD is the high purity and hardness. On the other hand, one of the main concerns of CVD is that waste gases are highly toxic. (9).In recent studies, ethylene in gaseous form was deposited on IR substrate via chemical vapour deposition to produce thin and highly pure graphene sheets. Other metals were used as substrates for monolayers of graphene films to grow on such as, Ru, Co, Ni, and alloys like Ni-Mo, and Co-Ni. (10).

3.2.2 Epitaxial growth on metal surfaces

Epitaxial growth of graphene on the surface of metals is investigated as a method that can overcome the limitations of other fabrication methods such as mechanical exfoliation. In such approach, the film structure, thickness and size can be controlled. This method is based on the formation of graphene on silicon carbide (SiC) which proceeds via the thermal desorption or sublimation of silicon from the SiC surface using for example electron irradiation. Subsequent graphitisation of the excess carbon atoms is left behind. Although this method provides a selected crystalline orientation, but it does not allow the growth of one-layer graphene. (6), (10), (11).

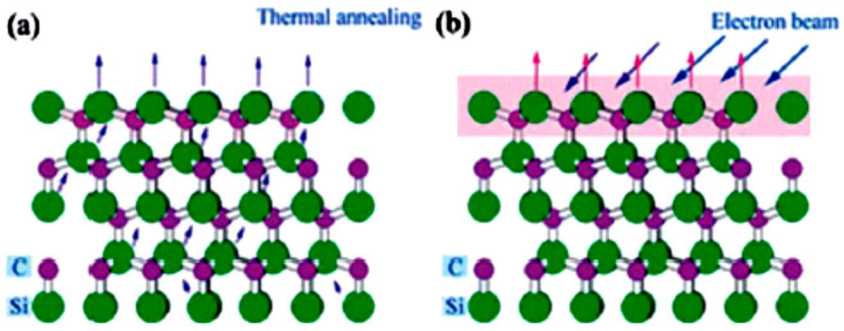

Fig 3.2: Schematic diagram of Si sublimation through (a) Annealing and (b) Electron irradiation. (10).

Top down approaches

3.2.3 Mechanical exfoliation

Graphene sheets can be prepared using mechanical exfoliation by scotch tape. Where Geim et al. have managed to produce 10 µm thick mono layers of graphene using microchemical cleavage. (6).

3.2.4 Liquid phase exfoliation

In such method, graphene is exfoliated in water or other solvent and a surfactant. Then, ultrasonication is used for the cleavage of graphene of its precursors. The basic idea of this technique is to exfoliate graphite oxide from aqueous layers of graphene oxide. This method is limited by the fact that the exfoliated graphene oxide needs further reduction to be electronically conductive. (7).

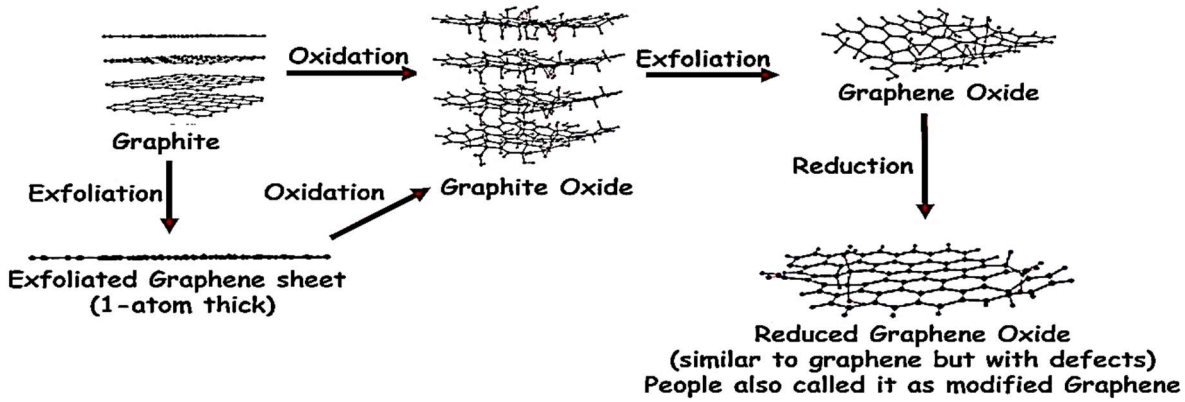

Fig 3.3: Process of Graphene exfoliation (8).

3.2.5 Hummer's method (Exfoliation and Chemical reduction of Graphite oxide)

The most-widely used method for obtaining graphene from exfoliation of graphite oxide is the so-called "Hummer's method". The need of an inexpensive and a highly yield method is the reason behind the distinction of Hummer's and Hummer's modified methods. In such approach, Graphite powder is used with oxidizing agents to form the graphite oxide. Then, such graphite oxide is exfoliated to obtain graphene oxide. To obtain functionalized graphene oxide, reduction is done by Hydrazine or other green methods as in our case. The term "functionalized graphene£ here refers to the incomplete reduction of graphene. But

Graphene oxide is electrically insulating due to the functional groups disrupting the sp2 hybridized layers, so efficient reduction is a crucial step in gaining back the electrical properties of the material. One of the key issues surrounding chemical reduction is that GO sheets upon reduction tend to aggregate and precipitate. (10).

Modified Hummer's method excludes $NaNo_3$ and uses phosphoric acid. This has proved to improve the oxidation process and electrical conductivity of the product. (12).

Attention has been recently drawn on the step of reducing the graphene oxide. Graphene oxide needs reduction in an attempt to restore the structural and electronic properties. Graphene conductivity is a function of the long-ranged conjugated layers of the honey comb lattice. Graphene functionalization breaks this chain and localizes the π electrons, which in turns leads to a decline in the carriers' mobility and concentration. Such attached functional groups act as scattering centres that blocks the pathway between sp^2 clusters. (13).

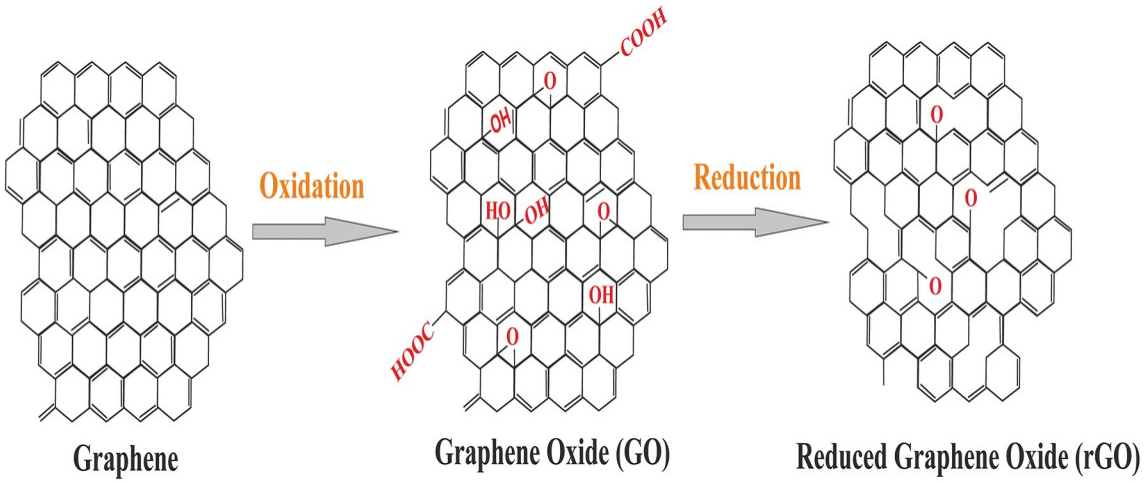

Fig 3.4: Graphite, graphite, graphene oxide and reduced graphene oxide difference in structure. (26).

3.3 Reduction strategies of Graphene oxide

3.3.1 Thermal annealing

In such strategy, Graphene oxide is reduced by applying rapid heating (>2000 c°) that helps exfoliating graphite oxide into graphene oxide, and at the same instant attaching the functionalized oxygen groups to carbon atoms to form CO or Co_2 gas between the stacked

layers. (14). This procedure makes it simple to produce graphene on a large scale. Notwithstanding, this method is effective just to deliver little size and wrinkled graphene sheets. This is because the decomposition of oxygen-containing functional groups expels carbon atoms from the carbon plane. This results in splitting of the graphene sheets into smaller pieces and leads to carbon plane distortion. (15).

Wang et al. Illustrated that electrical conductivity of reduced Graphene oxide depends on the annealing temperature. They showed that electrical conductivity of rGO at 500 c° was only 50 S/cm, but at a temperature of 700 and 1100 c° it reached 100 S/cm and 550 S/cm. (16).

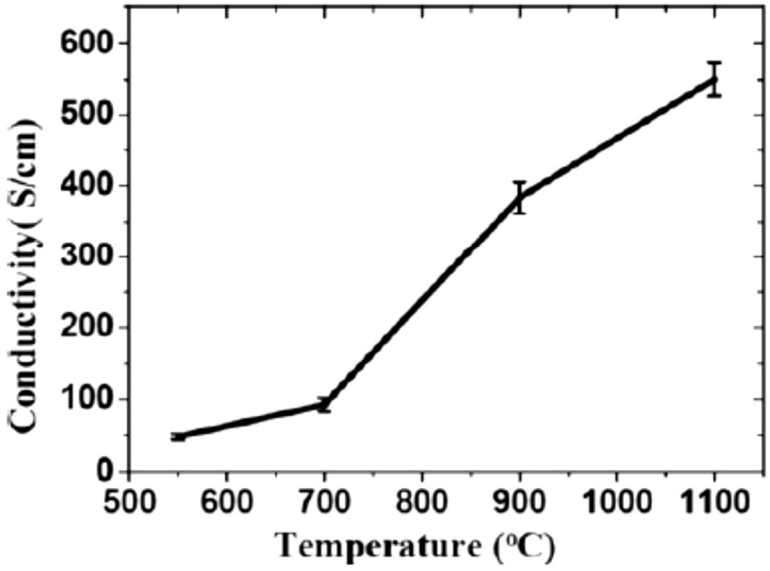

Fig 3.5: effect of increasing annealing temperature of reduced graphene oxide on the electrical conductivity. (16).

In addition to annealing temperature, one must take in mind the effect of annealing atmosphere on the reduction of GO. Wu et al. reported to use a mixture of Ar ang H_2 (1:1) ratio, this led to an increasing conductivity of 1000S/cm. Moreover, Li et al. reported annealing GO in low-pressure ammonia (2 Torr N_33/Ar (10% NH_3). This can produce simultaneous nitrogen doping and reduction of GO. Electrical measurements carried out proved that GO annealed in Ammonia had higher electrical conductivity than that annealed in H_2. (17).

3.3.2 Chemical reduction

3.3.2.1 Chemical reagent reduction

Using chemical reducing agents is a straight forward procedure. It requires moderate heat and carried out in normal laboratory conditions. This procedure makes reduction of graphene oxide easier for mass production.

3.3.2.1.1 Reduction by Hydrazine

Reduction by Hydrazine can be done by adding the reagent into dispersed GO. upon drying agglomerated graphene sheets are obtained. Reduction with Hydrazine yields conductivity ranging of 99.6 S/cm and carbon to oxygen level of 12.5. (18). Although hydrazine (N_2H_4) is considered a good reducing agent, but it has hazardous effect on humans and animals. According to the occupational safety and health guidelines on hydrazine, a person subject to 1.0 part of hydrazine per million parts of air (ppm) once a week for six months may develop fluid in chest cavity, bronchitis and in case of extensive exposure this may cause death. (19).

3.3.2.1.2 Reduction using metal hydrides

Metal hydrides such as Sodium hydride and lithium aluminium hydride have been proposed a s reducing agents, but unfortunately these hydrides have strong reactivity with water (the solvent of GO). Instead, $NaBH_3$ s was proposed as a reducing agent, but it is slowly hydrolysed in water and can only reduce the c=o. (20). Hydrogen Iodide (HI) was also proposed as a reducing agent. GO reduced by HI proved to have better flexibility and strength than Hydrazine reduced GO.. (21).

3.4 Reduction Mechanism

Reduction of graphene oxide aims at eliminating formed functional groups formed by oxidation process and restoring back the defects created as well as the structure. According to Li et al., conductivity of graphene monolayers is dependent on carrier transport between the sp^2 clusters pathways. Functional groups present on the planar side reduces electrical conductivity whilst those present on the edge have a less effect. (22). Reduction of graphene by thermal annealing can help convert epoxy groups into less stable hydroxyl groups. At temperature ranging between 700-1000 c° Hydroxyl groups can be removed. As for carbonyl groups, they are more stable than epoxy groups and can't be removed in annealing temperature less than 1700 c°. (23, 24).

Recovery of graphene conductivity is a must. This can be done by restoring the long range conjugated bonds of the sp^2 clusters. This is to provide a pathway for the electrons to be transported. According to Mattevi et al, sp^2 clusters are originally isolated and upon extensive reduction by annealing, defective areas are produced. Upon a threshold value new sp^2 domains are formed, and a minimum of 60 % sp^2 hybridization GO is considered conductive. (25).

3.5 Reduced graphene oxide as supercapacitor's electrode material

Meryl D. Stoller et al. Prepared chemically modified graphene and was used as a supercapacitor electrode material. In such approach, chemically modified graphene was synthesized by Hummer's method followed by suspending graphene oxide sheets in water followed by reducing them using hydrazine hydrate. Such method showed maximum specific capacitance f 135 F/g using 10 molar KOH. (27).Yao Chen et al. Reported the preparation of reduced graphene oxide using hydrobromic acid as a reducing agent. Electrolytes used were ionic liquids. Graphene oxide was prepared using Hummer's method. Followed by addition of 3 ml hydrobromic acid into the G colloids. Specific capacitance was measured in $BMIPF_6$ and $BMIBF_4$. Maximum capacitance was obtained using BMIBF4 as an organic electrolyte. Specific capacitance reached 74 F/g at a scan rate of 10 mV/s. (28).Chen et al. Proposed preparation of reduced graphene oxide by the aid of hydrobromic acid in aqueous electrolytes. Specific capacitance values reached 348 F/ g at a current density of 0.2 A/g. using sulphuric acid. (29).Zhang et al. proposed an environmentally friendly route to reduce graphene oxide. Glutathione as a reducing and stabilization agent has been used. The exfoliated GO was prepared using Hummer's method. Such agglomerated was dispersed in water and ammonia mixture in addition to 50 ml of GHS. The resultant RGO showed a maximum specific capacitance value of 140 F/g at a current density of 5A/g. (30). Jilia Zhang et al. testified using L-ascorbic acid as a reducing agent. GO was prepared using the normal procedures of Hummer's method. Further, 50 mg of L-ascorbic acid was added to 50 mL (0.1 mg mL) of an aqueous dispersion of the GO under stirring and reduction of GO was confirmed by FTIR. (31). Wei Lv et al. have synthetized low-temperature exfoliated graphene through vacuum-prompted exfoliation. Graphene oxide was prepared using Hummer's method followed by chemical exfoliation at a temperature ranging between 150 and 200 c°. Such heat treatment is accompanied is done in a low-pressure environment (< 1 Pa). Such high vacuum, accompanying the removal of the oxygen-based functional groups at a low temperature, results in the exfoliation of graphene layers. Maximum specific capacitance of 262 F/g was

reached at 1 mV/s using KOH as an electrolyte. (32).Yanwu et al. have prepared reduced graphene oxide platelets by exfoliating graphite oxide in propylene carbonate then reducing the resultant graphene oxide platelets using thermal reduction. Propylene carbonate was used as a solvent for exfoliation of graphene oxide platelets. Thermal reduction was used at 150 c° to remove the oxygen containing functional groups. Using $TEABF_4$ as an electrolyte, specific capacitance was calculated at 5 mA/g and reached 120 F/g. (33). Sliwak et al. have synthesised Nitrogen-doped reduced graphene oxide by hydrothermal method at 180 c°. Nitrogen species are pyridinic followed by amide/amine, pyrrolic, and quaternary nitrogen. Specific capacitance value was recorded to be 209 F/g at 20 A/g. (34). Several other techniques were used to dope and reduce graphene oxide by Nitrogen-based compounds. Lu et al. reported preparing Nitrogen- doped graphene sheets by chemical vapour deposition, which showed a surge in the concentration of charge carriers along with the growth temperature. (35). Xing et al. reported preparing 3D Nitrogen- doped Graphene oxide using melamine. Melamine was used as a reducing agent in the presence of ammonia. Using chronopotentiometry, specific capacitance value was 170.5 F g^{-1} at 0.2 A g^{-1} showing good electrochemical stability for high-performance supercapacitors. (36). Min and his co-workers have prepared Pyridinic–rich nitrogen-doped graphene nanoplatelets (PRGOs) via an acid–catalysed dehydration reaction using, GO and 3, 4-diaminopyridine. PRGOs show high performance as supercapacitors, electrochemical properties were characterized by chronopotentiometry, and the specific capacitance value reached 214 F/ g at current density of 0.1 A/g maintaining a long-term stability. (37). Xiaolin Li et al. proposed simultaneous functionalization and reduction of graphene oxide using annealing in ammonia. Graphene oxide sheets were prepared using modified Hummer's method. Reaction with ammonia was done by annealing in NH_3/Ar with a concentration of 10% ammonia at various temperatures that reached 1100 c° in an atmospheric pressure of 2 Torr. (38).Yong et al have prepared 3D macroscopic graphene hydrogels (MGHs) in a one-step hydrothermal reaction. Dispersions with 1,4-butanediamine acting as a nitrogen source. The specific capacitance value was268.8 F/g at 0.3 A /g in 6 M KOH electrolyte, and this capacitance could be maintained for 84.9%, although the discharging current density reached 10 A/ g. (39).Zhu et al. reported exfoliating and reduction of graphene oxide using a simple microwave- assisted method. GO powder prepared using modified Hummer's method were treated in a microwave oven at 700 W for 1 mi. Upon irradiating, the powder expanded dramatically. Reported specific capacitance value for such microwave reduced graphene oxide is 191 F/g at a constant current density of 150 mA/g. (40).Lee et al. Synthesized

RGO at low temperature and pressure using assisted-plasma. In such reduction method, in hydrogen gas was generated to remove oxygen functional groups from graphene oxide. Attention has been drawn to plasma treatment due to its low and efficiency in reduction of graphene oxide. (41).

Recently, light has been spotted on using alternative "green" reducing agents that are eco-friendly and efficient. Sodium borohydride, potassium hydroxide, benzyl alcohol, formic acid, and many other reducing agents have been proposed. (42).Yang and his co-workers reported preparing reduced graphene oxide using sodium borohydride and $CaCl_2$ as a catalyst. In such approach, graphene oxide was prepared using modified Hummer's method. For reduction $NaBH_4$ (2.28 g) and $CaCl_2$ (4.4 mg~1.78 g) was added to a 200 mL GO suspension then RGO was filtered and washed with DI water. (43).X Fan et al. have proposed preparing reduced graphene oxide using NaOH as a green and eco-friendly reducing agent. They suggested that exfoliated graphene oxide can undergo fast reduction in the presence of strong acidic medium. They relied on the fact that the higher the PH – the higher is the degree of deoxygenation. (44). Dreyer and his co-workers have manufactured reduced graphene oxide using benzyl alcohol (BnOH). A mixture of 200 % GO wt. in benzyl alcohol was heated for 24 h in a temperature of 100 c °. Specific capacitance value was 35 F/g. (45). Mitra et al. reduced GO using formic acid. Where 100 ml of formic acid was added to suspended GO and was kept at 100 c° for 18 h, 24 h and 30 h. Results have shown that most of the oxygen functional groups were removed of the Formic acid reduced graphene oxide mixture (FRGO) with the highest annealing time. (46).

3.6 Activated graphene oxide as a supercapacitor electrode material

Functionalization using covalent and non-covalent chemistry helps modulating intrinsic properties and activating graphene oxide. A wide range of activation materials have been used such as polymers, organic compounds, bio materials and so on. (48).

3.6.1 Functionalization with polymers

Mixing of graphene and polymers can be achieved via covalent and non-covalent bonding. Where the latter occurs because of the weak Van der wall attraction force. As for the covalent bonding, it involves strong bonding between the GO oxygen functional groups and the polymer's molecules. (49).Covalent bonding involves one of two methods named "grafting from" and "grafting to "Grafting from" method involves using

initiators at the surface of graphene followed by in situ surface initiation polymerization to produce polymer chains. According to Lee et al., a surface initiator (a-bromoisobutyryl bromide) is added to graphene to functionalize the hydroxyl groups, and other polymers were then added to induce polymer chains. (50).“Grafting to “method involves bonding functionalized polymer chains into graphene surface. This normally includes esterification and amidation between the amine and hydroxyl groups of the polymers and carboxylic groups in the GO. Grafting to method usually leads to enhanced mechanical and thermal properties of GO. (49).

3.6.2 Functionalization with Nano particles

Functionalization of GO-based nanocomposites provides excellent charge transport, high surface area and high catalytic activity. This decoration can be made via chemical or physical process. Such Nano particles include Pt, Au, Ag, Ru and other metal oxide-based Nano composites. (48). Dong and his co-workers proposed preparing Pt Nano particles on graphene sheets. GO was synthesized according to Hummer’s method and 1.5 ml of H_2PtCl_6 was added to the graphene oxide solution. Findings proved enhanced electrolytic activity of graphene activated with Pt Nano particles. (51).

Baby et al. demonstrated decorating graphene sheets with Nano crystalline Au. The Nanocomposite was prepared by magnetically stirring 0.2 g of purified graphene with 1 M $HAuCl_4 \cdot 3H_2O$ for 12 h. Results showed that metal nanoparticles act as spacers and prevents restacking of functionalized graphene. Cyclic voltammograms showed improved performance of the Au-RGO than bare reduced graphene oxide. (52). Bong et al. have prepared Pt -Ru Nano particles and loaded them into graphene using colloidal method. Electrochemical activity was determined cyclic voltammetry in a methanol as an oxidizing agent. (53).

3.6.3 Functionalization with organic compounds

Organic compounds’ functionalization with graphene oxide have drawn attention due to the solubility in water and other organic compounds. A wide range of organic compounds have been used to functionalize graphene oxide. Among which are ionic liquids, pyrene, methylene green and adenine. (49). Liu et al. reported using Methylene green -reduced graphene oxide nanocomposite. In this study, Methylene green was used to non-covalently

functionalize Hummer's prepared reduced graphene oxide. Results showed that Methylene green prevented aggregation of GO as well as improving electrochemical activity. (54).

El-Gendy et al. have demonstrated preparing spongy adenine functionalized graphene oxide through 3D network crinkly sheets. In such approach, Graphene oxide was synthesized using modified Hummer's method and functionalization of graphene oxide was done via adenine. Electrochemical performance was evaluated, and specific capacitance of the adenine functionalized graphene reached 323 F/g at a current density of 1 A/g. This high specific capacitance value is attributed to the addition nucleophilic reactions between $–NH_2$ adenine groups and carboxylic acid or epoxy groups on the Graphene surface. (55).

3.7 Graphene/Metal oxides composite electrode materials

As discussed in previous sections, Graphene based electrode materials contribute in double layer capacitance via physical electrostatic interaction at both electrodes-electrolyte surfaces. Graphene is extensively used because of its chemical stability, excellent mechanical properties, high surface area and fast charge transport. However, graphene-based supercapacitor electrodes have limited capacitance values thus it was logical to combine metal oxides with graphene-based materials to construct hybrid electrodes. Metal oxides are known to contribute to pseudo capacitance by the rapid redox reactions occurring at the electrode-electrolyte interface. In addition, this combination of pseudo capacitance and double layer capacitance materials leads to better chemical stability and specific capacitance values. (56).

3.7.1 Graphene/Ruthenium oxide-based electrode materials

Sanguen et al. proposed preparing RuO_2/graphene thin film with excellent stability and specific capacitance value. In such approach, RuO_2 is fabricated on graphene coated cu foil by electroplating method. This composite electrode showed excellent specific capacitance value of 1561 F/g at a scan rate of 5 mv/s as well as superior capacitance retention of 98 %. (57). Thangappan et al. have synthesized Ruo2/GO Nanocomposite using hydrothermal method. GO was prepared using modified Hummer's method. Electrochemical performance was tested using cyclic voltammetry with excellent specific capacitance value of 441 F/g at a current density 0.1 A/g. (58).Yang et al. Prepared a 3D porous framework of RuO2/reduced graphene oxide hydrogels (RuO_2/RGOH) using hydrothermal method. GO was prepared using modified Hummer's method and 3.5 ml of $RuCl_3$ was added to the GO solution by the aid of NaOH to neutralize the PH value of the dispersion. Specific capacitance value was measured to be 345 F/g at 1 A/g. Excellent cyclic stability was observed even after the 2000^{th} with a high retention of 95 %. (59). Zhang and co-workers have prepared asymmetric supercapacitor using ruthenium oxide and reduced graphene oxide. GO was prepared using Modified Hummer's method followed by reduction in microwave oven followed by deposition of RuO_2 nanoparticles on the reduced graphene oxide sheets. Capacitance value of the asymmetric electrode reached 357 F/g at a current density of 0.3 A/g. This high capacitance value is attributed to the broadened potential value by the aqueous electrolyte. (60).

3.7.2 Graphene/Manganese oxide-based electrode materials

Jadhav et al. have reported preparing MnO_2 nanorods by hydrothermal oxidation on graphene surface. In such experiment, graphene oxide was prepared using modified Hummer's method followed by reduction in Hydrazine Hydrate. MnO2-rGO composite was prepared by adding $MnSO_4.H_2O$ to KMnO4 a and 0.1 g of dispersed graphene powder. The mixture was then treated via hydrothermal method. Highest recorded value for specific capacitance was 759 F/g at a current density of 2 A/g. (61). Singu and co-workers used one pot in-situ chemical synthesis method to prepare exfoliated reduced graphene oxide-manganese oxide nanocomposites. Graphene oxide was synthesised using modified Hummer's method and 0.63 g of $MnCl_2$ was added to GO solution then heated for 4h at 70°c. Specific capacitance of the rGO-MnOx was found to be 398.8 F/g at a scan rate of 100 mV/s.This relatively high specific capacitance value is due to the high surface area of the nanocomposite. (62). Wu et al. have reported preparing Mn_3O_4/graphene nanocomposites by solvothermal method. In such approach GO was prepared using modified Hummer's method and 0.5 ml−1 homogeneous GO suspension was added to 0.0027 mol of $Mn(AC)_2 \cdot 4H_2O$ followed by treatment via hydrothermal method. Highest specific capacitance value was 225 F/ g at a scan rate of 5 mV/s 1 M Na_2SO_4 electrolyte with excellent capacitance retention. (63). Ghasemi et al. proposed preparing MnO_2 /RGO using sonochemical method. GO was prepared using modified Hummer's method. Irradiation of 0.50 M $KBrO_3$ and 0.25 molar Mn $(CH3COO)_2$ using a 20 kHz ultrasound horn transducer system to synthesize MnO. An electrostatic coprecipitation method was applied to anchor MnO2 nanoparticles on GO sheets. Maximum specific capacitance value was found to reach 344 F/g at a scan rate of 5mv/s. (64).Jinyang Dong et al. have prepared Nitrogen-doped Graphene Flower-like MnO_2 Nanocomposite by hydrothermal method. Nitrogen-doped graphene (NG) was prepared by adding 60 mL of GO solution into a two-necked flask. 0.5 g of urea under stirring. This was followed by heating for 12 h at 95°c. Hybrids of NG-MnO_2 were prepared by adding 10 mg of dispersed GO, 316 mg of $KMnO_4$ and 1 g of urea. This mixture was then transferred to autoclave and heated at 120 °C for 12 h. Maximum specific capacitance value obtained at 0.5 A/g was 220 F/g. (65).

3.7.3 Graphene/Cobalt oxide-based electrode materials

Huan-Wen Wang et al. have demonstrated preparing reduced graphene oxide/cobalt oxide composites as electrode materials for supercapacitors by chemical precipitation approach. GO was prepared using modified Hummer's method. GO/Co $(OH)_2$ composites of different mass ratios were prepared. 0.1 mg of dispersed GO was added to dissolved 1.45 g of $CoCl_2 \cdot 6H_2O$ then $NH_3 \cdot H_2O$ was added to the solution. Thermal treatment of the products was performed at 60°C for 12 h. Specific capacitance value of the composite reached 291 F/g at 1 A/g current density. Also, the composite exhibited excellent capability rate of 88% between starting 1 A/g till 8 A/g. Moreover, the composite maintained 90% of the initial value over 1000 cycles. (66). Nguyen et al. synthesized reduced graphene oxide sheets decorated with cobalt oxide nanoparticles using hydrothermal method. GO was prepared using improved Hummer's method followed by freeze drying. Co_3O_2/rGO composite was prepared by mixing 0.01 g of GO and 0.10 g of Co $(NO_3)_2.6H_2O$followed by the addition of 0.5 ml of NH_4OH, then the mixture was transferred into an autoclave for 48 h at 100°C. Specific capacitance value of Co_3O_4/rGO was 545 F/g at current density of 8 A/g. This high specific capacitance value is due to the faradic capacitance nature of the composite as well as the outstanding electronic conductivity offered by rGO. (67).Xiao-Chen Dong, and co-workers proposed preparing 3D graphene-cobalt oxide electrode using hydrothermal procedure. GO was prepared using chemical vapour deposition (CVD) using Ni foam as a substrate. The Graphene/Co_3O_4 Nanowire Composite was prepared by dissolving of $CoCl_2.6H_2O$ in 20 mL of water followed by immersing of the graphene grown on Ni foam into the solution. Finally, the sample was heated at 450 °C for 2h. Specific capacitance of such electrode reached 768 F/g at a current density of 10 A/g. (68). Naveen et al. prepared (Co3O4)/graphene nanosheets composites. GO was prepared using modified Hummer's method. Exfoliation of GO was done in a muffle furnace at moderate temperature of 150°C. 10 mM of cobaltous nitrate was added to dispersed 50 ml of GO. 12 mM of urea was then added and finally the solution was heated at 120°C. Results showed that the highest value of specific capacitance of 650 F/g at a scan rate of 5mv.Such high specific capacitance value is due to the faradic nature of cobalt along with the high electronic conductivity of graphene. (69).

3.8 Graphene/metal sulphides-based electrode materials

Xing et al. have proposed synthesise of Nickel sulphide/reduced graphene oxide nanocomposite using an environmentally friendly reducing agent. According to the authors, GO was prepared using modified Hummer's method. 0.3 mM $NiCl_2 \cdot 6H_2O$ was added to dissolved GO in addition to l-cysteine (reducing agent and sulphur donor). This mixture was moved into an autoclave and was hydrothermally treated for 6 h at 160 °C. Electrochemical measurements revealed excellent specific capacitance value of 1169 F/g at a current density of 5 A/g as well as good stability at the 1000th cycle. The outstanding supercapacitive performance of such composite is attributed to high conductivity of reduced graphene oxide and sulphur. In addition, anchored Nis nanoparticles on graphene nanosheets makes the whole composite more stable.

Huang and co-workers reported synthesizing reduced graphene oxide /copper sulphide as an electrode for supercapacitors. GO was prepared according to modified Hummer's method. The rGO wrapped CuS hollow spheres were synthesised by adding dissolved Cu $(NO_3).3H_2O$, thiourea to rGO using hydrothermal reaction for 20 h at 180°C.Specific capacitance of the composite was measured to be 2317 F/g at a current density of 1 A/s.This high supercapacitance value is due to the high conductivity and capacitance of copper, large surface area and conductive networks of the CuS/rGO.(71). Ramachandran et al. have prepared Zinc sulphide decorated graphene nanocomposites by a solvothermal approach. GO was prepared using modified Hummer's method. ZnS/Graphene composite was prepared by adding 0.075 M of ethylenediamine and 0.136 ml of carbon disulphide (CS_2) to 10 mg of dissolved GO. After stirring the composite was transferred into an autoclave and heated for 12 h at 180°C.Specific capacitance value of such composite reached 197.1 F/g. (72).Ratha et al. prepared Layered Tungsten Disulphide Reduced Graphene Oxide by hydrothermal method. GO was prepared by the well-known modified Hummer's method and further reduction was done via hydrothermal method.WS_2 sheets were synthesised by adding 3 mM WCl_6 ,15 mM thioacetamide and 5 mg/mL GO solution were kept in the hydrothermal reactor for 24 h at 265°C.Highest specific capacitance observed for the composite was 350 F/g at a scan rate of 2 mV/s. The admirable capacitive characteristics are due to the high electrical conductivity, fast transport of electrolyte ions and pseudo capacitive nature of WS_2. (72).

Firmiano et al. proposed preparing bonded 2D MoS_2 on Reduced Graphene Oxide to use as s supercapacitor electrode. GO was prepared by modified Hummer's method. Synthesis of MoS 2 /RG was carried in a glove box and was then carried into microwave oven reactor for reduction. Specific capacitance value of this composite was 1558 F/g at 10 mV/s scan rate. (74). Cai et al. reported preparing $NiCo_2S_4$ grown on graphene fibres to use as electrode material for supercapacitors. Go was first prepared using modified Hummer's method. Fabrication of the graphene nanofiber was done by mixing GO along with ascorbic acid in water bat inside a silicon tube. Finally decorating GFs was done by coating it with $NiCo_2S_4$ in a hydrothermal reactor for 24 h at 180°C. volumetric capacitance of GF/$NiCo_2S4$ was up to 388 F cm−3 at a scan rate of 2 mV/s. (75) Meng et al. proposed preparing Cobalt Sulfide/Graphene Composite hydrogel to be utilized as a supercapacitor electrode material. GO was prepared using modified Hummer's method. Feeding ratios of Co $(CH3COO)_2 \cdot 4H_2O$ was added to GO. Sulphur were thiourea and ethanediamine. The whole mixture was treated hydrothermally for 12 h at 180°C.Maximum specific capacitance obtained was 564 F/g at a scan rate of 1 A/g. The hydrogel was characterized by the high capacity retention and stability of 94.8 % after the 1000th cycle. The specific capacitance value is related to unique nanostructure of the CoS interconnected with GO, which prevents restacking of graphene. Addition of CoS have facilitated electrolyte ion transferring as well as contributing to pseudo capacitance. (76). Xu et al. reported preparing cobalt sulphide/reduced graphene oxide composites as electrode material for supercapacitors. In such attempt GO was prepared using modified Hummer's method then 1 mmol of $CoCl_2 \cdot 6H_2O$ was added to dissolved GO. 0.5 mM of Sulphur source (sodium thiosulfate), and hydrazine hydrate was added to the solution and was treated hydrothermally at 180 °C for 12 h. Specific capacitance value of the composite reached 550 F/g at a current density of 1 A/g. The admirable value of specific capacitance is a result of the synergetic effect of both CoS ang rGO. In addition, the CoS particles prevented agglomeration and restacking of GO sheets, they also added porosity and allowed for electrolyte ion diffusion and transport within the composite. (77).

3.9 Metal oxides used as supercapacitor electrodes

Metal oxides, transition metal oxides, polymers and metal sulphides are utilized in pseudo capacitors due to their redox nature which enables fast reversible reactions. In addition, they possess high capacitance values and high energy density. Among the commonly used metal oxides are Ruthenium oxide, Manganese oxide and Nickel oxide.

Kim et al. proposed preparing Ruthenium dioxide nanotubes and utilized it as an electrode material. In such approach, Synthesis was done via microwave-hydrothermal process, where 1.0 g of $RuCl_3 \cdot nH_2O$ was added to 100 mL of a 10 M NaOH aqueous solution. This solution was then heated in a microwave system for 10 mins at 200 °C then was treated hydrothermally at the same temperature for 4 electrochemical measurements were measured, and a maximum specific capacitance value of 501 F/g was reached at a scan rate of 0.5 A/g. This excellent electrochemical performance is related to accessibility of electrolyte ions to the interior of the tubes and hence resulting in the rapid mass transport of H+ ions to electrochemically active sites. (78). Sarkar et al. have reported preparing manganese oxide films as an electrode material for electrochemical applications. Preparing of manganese oxide films was done via post chemical bath oxidation annealing on stainless steel sheet. Maximum specific capacitance measured was 410.5 A/g at a current density of 0.46 A/g. (79). Pei et al. prepared NiO via hydrothermal method to utilize as a supercapacitor electrode material. Synthesis process was as follows: 1.188 g $NiCl_2$ 6H2O and 0.200 g NaOH were dissolved in 30 ml ethanol then the solution was transferred into an autoclave and hydrothermally treated for 24 h at 120°C. This was followed by calcination at 300 °C. Electrochemical characterization was done in 6 M KOH which revealed an admirable specific capacitance value of 1046 F/g at a current density of 1.8 A/g. This high value of capacitance is credited to the fast-redox reactions which enhanced the transport of ions and electrons at the electrode/electrolyte interface. However, capacitance retention was 58.3 % after the 1000th cycle. (80). Kandalkar et al. proposed preparing cobalt oxide thin films and utilized it as an electrode material. In this approach, cobalt oxide thin film was synthesized from cobalt chloride precursor ($CoCl_26H_2O$) by ionic layer adsorption and reaction on surface of copper substrate. Maximum Specific capacitance value was 165 F/g at 50 mV/s. (81). Juan Xu et al. have prepared cobalt oxide nanotubes as a supercapacitor electrode material. Preparing of Co_3O_4 nanotubes was done

via chemically depositing cobalt hydroxide in anodic aluminium oxide. This was followed by annealing in 500°C.Specific capacitance value was 574 F/g at a current density of 0.1 A/s.This high capacitance value is related to the morphology of the prepared nanotubes which provides large specific surface area. Such surface area helps to enlarge the contact area between electrode and electrolyte and enhance the surface adsorption/desorption process of alkaline electrolyte ions. (82).

3.10 Metal sulphides used as electrode materials

Chen et al. have reported preparing nanosheet arrays of electrodeposited Nickel Cobalt Sulphide. The Ni-Co-S was electrochemically co-deposited onto carbon cloth. The electrodeposition solution contains 5 mM $CoCl_2$ .6 H_2O along with of $NiCl_2$. $6H_2O$ and thiourea. The NI-Co-S was used as a positive electrode in an asymmetric supercapacitor configuration where the other negative electrode was graphene-based. Specific capacitance value of the electrode was measured to be 1445 F/g at a current density of 10 A/g. (83).Yang et al. have reported the Solvothermal synthesis of hierarchical flower-like b-NiS. Preparing of the NiS was done via facile solvothermal method. In such approach, diethanolamine (H_2DEA) was used as a coordination agent and a solvent for the prepared architecture. $NiCl_2$ and thiourea were used and an amount of H_2DEA was used. The mixture was hydrothermally treated for 12 h at 180°C. Specific capacitance values recorded showed specific capacitance of 457 F/g at a current density of 2 A/g. Such admirable specific capacitance value is related to the unique configuration which shortens the diffusion path of the electrolyte ions. In addition, the surface area offers more accessible sites for the electrolyte ions. (84). Krishnamoorthy et al. synthesised Ruthenium sulphide nanoparticles by sonochemical method. In such approach, thiourea was the sulphur source where it was added to RuCl with the aid of Argon purging. The mixture was then subject to ultrasound radiation for 2 h using titanium horn and showed specific capacitance of 85 F/g at a current density of 0.1 A/g. (85). Ting Zue et al. have prepared CuS nanoneedles on a CNT using template-engaged chemical conversion route as a supercapacitor electrode material. Maximum specific capacitance value reported was 110 F/g at a current density of 2.9 A/g. The nanoneedles also showed an excellent stability of 100 % after the 1000th cycle because of the presence of the carbon nanotubes which served as a supporter for the CuS. (86). Zusing Yang and his co-workers have reported preparing hollow cobalt sulfide hexagonal

nanosheets as an electrode material. Co $(NO_3)_2$ (0.291 g),0.15 g of sulphur source (thioacetamide) and PVP (0.07 g) were added to ultrapure H2O. This was followed by the addition of 0.5 M NaOH. The whole solution was then heated for 1 h at 100°C.Maximum specific capacitance value was 326.4 F/g. (87).

References:

1-Georgakilas, V., Perman, J. A., Tucek, J., & Zboril, R. (2015). Broad Family of Carbon Nanoallotropes: Classification, Chemistry, and Applications of Fullerenes, Carbon Dots, Nanotubes, Graphene, Nanodiamonds, and Combined Superstructures. Chemical Reviews,115(11), 4744-4822. doi:10.1021/cr500304f

2- Dreyer, D. R., Park, S., Bielawski, C. W., & Ruoff, R. S. (2010). The chemistry of graphene oxide. Chem. Soc. Rev.,39(1), 228-240. doi:10.1039/b917103g

3- CHUNG, D. D. (2002). Review Graphite. JOURNAL OF MATERIALS SCIENCE,37, 1475-1489.

4- Geim, A. K. (n.d.). The rise of graphene. Nature Materials,6, 183-191.

5- Rao, C. N., Sood, A. K., Subrahmanyam, K. S., & Govindaraj, A. (2009). ChemInform Abstract: Graphene: The New Two-Dimensional Nanomaterial. ChemInform,40(52). doi:10.1002/chin.200952249

6- Zhang, L. L., Zhou, R., & Zhao, X. S. (2010). Graphene-based materials as supercapacitor electrodes. Journal of Materials Chemistry,20(29), 5983. doi:10.1039/c000417k

7- Hou, J., Shao, Y., Ellis, M. W., Moore, R. B., & Yi, B. (2011). Graphene-based electrochemical energy conversion and storage: Fuel cells, supercapacitors and lithium ion batteries. Physical Chemistry Chemical Physics,13(34), 15384. doi:10.1039/c1cp21915d

8- What is difference between graphene oxide and exfoliated ... (n.d.). Retrieved from https://www.researchgate.net/post/What_is_difference_between_graphene_oxide_and_exfoliated_graphite

9- Graphene News. (n.d.). Retrieved from https://www.graphenea.com/blogs/graphene-news?page=9

10- Edwards, R. S., & Coleman, K. S. (2013). ChemInform Abstract: Graphene Synthesis. Relationship to Applications. ChemInform,44(13). doi:10.1002/chin.201313233

11- Tan, Y. B., & Lee, J. (2013). Graphene for supercapacitor applications. Journal of Materials Chemistry A,1(47), 14814. doi:10.1039/c3ta12193c

12- Marcano, D. C., Kosynkin, D. V., Berlin, J. M., Sinitskii, A., Sun, Z., Slesarev, A., . . . Tour, J. M. (2010). Improved Synthesis of Graphene Oxide. ACS Nano,4(8), 4806-4814. doi:10.1021/nn1006368

13- Hun, S. (2011). Thermal Reduction of Graphene Oxide. Physics and Applications of Graphene - Experiments. doi:10.5772/14156

14- Zhao, J., Pei, S., Ren, W., Gao, L., & Cheng, H. (2010). Efficient Preparation of Large-Area Graphene Oxide Sheets for Transparent Conductive Films. ACS Nano,4(9), 5245-5252. doi:10.1021/nn1015506

15- Schniepp, H. C., Li, J., Mcallister, M. J., Sai, H., Herrera-Alonso, M., Adamson, D. H., . . . Aksay, I. A. (2006). Functionalized Single Graphene Sheets Derived from Splitting Graphite Oxide. The Journal of Physical Chemistry B,110(17), 8535-8539. doi:10.1021/jp060936f

16- Wang, X., Zhi, L., & Müllen, K. (2008). Transparent, Conductive Graphene Electrodes for Dye-Sensitized Solar Cells. Nano Letters,8(1), 323-327. doi:10.1021/nl072838r

17- L. X. (2009). simultaneous nitrogen doping and reduction of graphene oxide. J Am Chem Soc.,43.

18- Fernández-Merino, M. J., Guardia, L., Paredes, J. I., Villar-Rodil, S., Solís-Fernández, P., Martínez-Alonso, A., & Tascón, J. M. (2010). Vitamin C Is an Ideal Substitute for Hydrazine in the Reduction of Graphene Oxide Suspensions. The Journal of Physical Chemistry C,114(14), 6426-6432. doi:10.1021/jp100603h

19- "Occupational Safety and Health Guideline for Hydrazine - Potential Human Carcinogen. (n.d.). Retrieved March 13, 2019, from https://www.cdc.gov/niosh/docs/81-123/pdfs/0329.pdf

20- Shin, H., Kim, K. K., Benayad, A., Yoon, S., Park, H. K., Jung, I., . . . Lee, Y. H. (2009). Efficient Reduction of Graphite Oxide by Sodium Borohydride and Its Effect on Electrical Conductance. Advanced Functional Materials,19(12), 1987-1992. doi:10.1002/adfm.200900167

21- Pei, S., Zhao, J., Du, J., Ren, W., & Cheng, H. (2010). Direct reduction of graphene oxide films into highly conductive and flexible graphene films by hydrohalic acids. Carbon,48(15), 4466-4474. doi: 10.1016/j.carbon.2010.08.006

22- Li, D., Müller, M. B., Gilje, S., Kaner, R. B., & Wallace, G. G. (2008). Processable aqueous dispersions of graphene nanosheets. Nature Nanotechnology,3(2), 101-105. doi:10.1038/nnano.2007.451

23- Gao, X., Jang, J., & Nagase, S. (2009). Hydrazine and Thermal Reduction of Graphene Oxide: Reaction Mechanisms, Product Structures, and Reaction Design. The Journal of Physical Chemistry C,114(2), 832-842. doi:10.1021/jp909284g

24- Xu, S. C., Ire, S., Musaev, D. G., & Lin, M. C. (2006). Quantum Chemical Study of the Dissociative Adsorption of OH and H2O on Pristine and Defective Graphite (0001) Surfaces: Reaction Mechanisms and Kinetics. The Journal of Physical Chemistry C,111(3), 1355-1365. doi:10.1021/jp066142i

25- Mattevi, C., Eda, G., Agnoli, S., Miller, S., Mkhoyan, K. A., Celik, O., . . . Chhowalla, M. (2009). Evolution of Electrical, Chemical, and Structural Properties of Transparent and Conducting Chemically Derived Graphene Thin Films. Advanced Functional Materials,19(16), 2577-2583. doi:10.1002/adfm.200900166

26- Ray, S. C. (2015). Application and Uses of Graphene Oxide and Reduced Graphene Oxide. Applications of Graphene and Graphene-Oxide Based Nanomaterials,39-55. doi:10.1016/b978-0-323-37521-4.00002-9

27- Stoller, M. D., Park, S., Zhu, Y., An, J., & Ruoff, R. S. (2008). Graphene-Based Ultracapacitors. Nano Letters,8(10), 3498-3502. doi:10.1021/nl802558y

28- Chen, Y., Zhang, X., Zhang, D., Yu, P., & Ma, Y. (2011). High performance supercapacitors based on reduced graphene oxide in aqueous and ionic liquid electrolytes. Carbon,49(2), 573-580. doi: 10.1016/j.carbon.2010.09.060

29- High performance supercapacitors based on reduced graphene oxide in aqueous and ionic liquid electrolytes

30- Zhang, D., Zhang, X., Chen, Y., Wang, C., & Ma, Y. (2012). An environment-friendly route to synthesize reduced graphene oxide as a supercapacitor electrode material. Electrochimica Acta,69, 364-370. doi: 10.1016/j.electacta.2012.03.024

31- Khosroshahi, Z., Kharaziha, M., Karimzadeh, F., & Allafchian, A. (2018). Green reduction of graphene oxide by ascorbic acid. doi:10.1063/1.5018941

32- Lv, W., Tang, D., He, Y., You, C., Shi, Z., Chen, X., . . . Yang, Q. (2009). Low-Temperature Exfoliated Graphenes: Vacuum-Promoted Exfoliation and Electrochemical Energy Storage. ACS Nano,3(11), 3730-3736. doi:10.1021/nn900933u

33- Zhu, Y., Stoller, M. D., Cai, W., Velamakanni, A., Piner, R. D., Chen, D., & Ruoff, R. S. (2010). Exfoliation of Graphite Oxide in Propylene Carbonate and Thermal Reduction of the Resulting Graphene Oxide Platelets. ACS Nano,4(2), 1227-1233. doi:10.1021/nn901689k

34- Śliwak, A., Grzyb, B., Díez, N., & Gryglewicz, G. (2017). Nitrogen-doped reduced graphene oxide as electrode material for high rate supercapacitors. Applied Surface Science,399, 265-271. doi: 10.1016/j.apsusc.2016.12.060

35- Lu, Y., Lo, S., Lin, J., Zhang, W., Lu, J., Liu, F., . . . Li, L. (2013). Nitrogen-Doped Graphene Sheets Grown by Chemical Vapor Deposition: Synthesis and Influence of Nitrogen Impurities on Carrier Transport. ACS Nano,7(8), 6522-6532. doi:10.1021/nn402102y

36- Xing, L., Hou, S., Zhou, J., Zhang, J., Si, W., Dong, Y., & Zhuo, S. (2015). Three-dimensional nitrogen-doped graphene aerogels functionalized with melamine for multifunctional applications in supercapacitors and adsorption. Journal of Solid-State Chemistry,230, 224-232. doi: 10.1016/j.jssc.2015.07.009

37- Lee, M. S., Choi, H., Baek, J., & Chang, D. W. (2017). Simple solution-based synthesis of pyridinic-rich nitrogen-doped graphene nanoplatelets for supercapacitors. Applied Energy,195, 1071-1078. doi: 10.1016/j.apenergy.2016.07.107

38- Barman, B. K., & Nanda, K. K. (2014). Hexamethylenetetramine mediated simultaneous nitrogen doping and reduction of graphene oxide for a metal-free SERS substrate. RSC Adv.,4(83), 44146-44150. doi:10.1039/c4ra08787a

39- Zhang, Y., Wen, G., Gao, P., Bi, S., Tang, X., & Wang, D. (2016). High-performance supercapacitor of macroscopic graphene hydrogels by partial reduction and nitrogen doping of graphene oxide. Electrochimica Acta,221, 167-176. doi: 10.1016/j.electacta.2016.10.115

40- Zhu, Y., Murali, S., Stoller, M. D., Velamakanni, A., Piner, R. D., & Ruoff, R. S. (2010). Microwave assisted exfoliation and reduction of graphite oxide for ultracapacitors. Carbon,48(7), 2118-2122. doi: 10.1016/j.carbon.2010.02.001

41- Lee, S. W., Mattevi, C., Chhowalla, M., & Sankaran, R. M. (2012). Plasma-Assisted Reduction of Graphene Oxide at Low Temperature and Atmospheric Pressure for Flexible Conductor Applications. The Journal of Physical Chemistry Letters,3(6), 772-777. doi:10.1021/jz300080p

42- Aunkor, M. T., Mahbubul, I. M., Saidur, R., & Metselaar, H. S. (2016). The green reduction of graphene oxide. RSC Advances,6(33), 27807-27828. doi:10.1039/c6ra03189g

43- Zhu, Y., Stoller, M. D., Cai, W., Velamakanni, A., Piner, R. D., Chen, D., & Ruoff, R. S. (2010). Exfoliation of Graphite Oxide in Propylene Carbonate and Thermal Reduction of the Resulting Graphene Oxide Platelets. ACS Nano,4(2), 1227-1233. doi:10.1021/nn901689k

44- Fan, X., Peng, W., Li, Y., Li, X., Wang, S., Zhang, G., & Zhang, F. (2008). Deoxygenation of Exfoliated Graphite Oxide under Alkaline Conditions: A Green Route to Graphene Preparation. Advanced Materials,20(23), 4490-4493. doi:10.1002/adma.200801306

45- Dreyer, D. R., Murali, S., Zhu, Y., Ruoff, R. S., & Bielawski, C. W. (2011). Reduction of graphite oxide using alcohols. J. Mater. Chem.,21(10), 3443-3447. doi:10.1039/c0jm02704a

46- Mitra, M., Chatterjee, K., Kargupta, K., Ganguly, S., & Banerjee, D. (2013). Reduction of graphene oxide through a green and metal-free approach using formic acid. Diamond and Related Materials,37, 74-79. doi: 10.1016/j.diamond.2013.05.003

48- D. C. (2012). Graphene Oxide: Preparation, Functionalization, and Electrochemical Applications. Chemical Reviews.

49- Zheng, W., Shen, B., & Zhai, W. (2013). Surface Functionalization of Graphene with Polymers for Enhanced Properties. New Progress on Graphene Research. doi:10.5772/50490

50- Lee, S. H., Dreyer, D. R., An, J., Velamakanni, A., Piner, R. D., Park, S., . . . Ruoff, R. S. (2010). Polymer Brushes via Controlled, Surface-Initiated Atom Transfer Radical

Polymerization (ATRP) from Graphene Oxide. Macromolecular Rapid Communications,31(3), 281-288. doi:10.1002/marc.200900641

51- Zhou, Q., Wang, G. C., Yang, L., Yang, Y., & Xu, Y. (2013). Carboxylic Graphene-Supported Platinum and Platinum-Palladium Nanoparticles with High Electrocatalytic Activity for Methanol Oxidation. Applied Mechanics and Materials,320, 670-674. doi: 10.4028/www.scientific.net/amm.320.670

52- Baby, T. T., Aravind, S. J., Arockiadoss, T., Rakhi, R., & Ramaprabhu, S. (2010). Metal decorated graphene nanosheets as immobilization matrix for amperometric glucose biosensor. Sensors and Actuators B: Chemical,145(1), 71-77. doi: 10.1016/j.snb.2009.11.022

53- Meeying, S., Viravathana, P., Wongchaisuwat, A., & Tangbunsuk, S. (2015). Synthesis and Characterization of PdCoNi Nanocomposites Supported on Graphene as Anodic Electrocatalysts for Methanol Oxidation in Direct Methanol Fuel Cell. Key Engineering Materials,658, 190-194. doi: 10.4028/www.scientific.net/kem.658.190

54- Liu, H., Gao, J., Xue, M., Zhu, N., Zhang, M., & Cao, T. (2009). Processing of Graphene for Electrochemical Application: Noncovalently Functionalize Graphene Sheets with Water-Soluble Electroactive Methylene Green. Langmuir,25(20), 12006-12010. doi:10.1021/la9029613

55- El-Gendy, D. M., Ghany, N. A., Sherbini, E. E., & Allam, N. K. (2017). Adenine-functionalized Spongy Graphene for Green and High-Performance Supercapacitors. Scientific Reports,7(1). doi:10.1038/srep43104

56- Yu, Z., Tetard, L., Zhai, L., & Thomas, J. (2015). Supercapacitor electrode materials: Nanostructures from 0 to 3 dimensions. Energy & Environmental Science,8(3), 702-730. doi:10.1039/c4ee03229b

57- Cho, S., Kim, J., Jo, Y., Ahmed, A. T., Chavan, H., Woo, H., . . . Im, H. (2017). Bendable RuO2/graphene thin film for fully flexible supercapacitor electrodes with superior stability. Journal of Alloys and Compounds,725, 108-114. doi: 10.1016/j.jallcom.2017.07.135

58- Thangappan, R., Arivanandhan, M., Kumar, R. D., & Jayavel, R. (2018). Facile synthesis of RuO 2 nanoparticles anchored on graphene nanosheets for high performance

composite electrode for supercapacitor applications. Journal of Physics and Chemistry of Solids,121, 339-349. doi: 10.1016/j.jpcs.2018.05.049

59- Yang, Y., Liang, Y., Zhang, Y., Zhang, Z., Li, Z., & Hu, Z. (2015). Three-dimensional graphene hydrogel supported ultrafine RuO2 nanoparticles for supercapacitor electrodes. New Journal of Chemistry,39(5), 4035-4040. doi:10.1039/c5nj00062a

60- Zhang, J., Jiang, J., Li, H., & Zhao, X. S. (2011). A high-performance asymmetric supercapacitor fabricated with graphene-based electrodes. Energy & Environmental Science,4(10), 4009. doi:10.1039/c1ee01354h

61- Ghosh, D., Giri, S., Dhibar, S., & Das, C. K. (2014). Reduced Graphene Oxide/Manganese Carbonate Hybrid Composite: High Performance Supercapacitor ElectrodeMaterial. ElectrochimicaActa,147,557-564. doi: 10.1016/j.electacta.2014.09.130

62- Singu, B. S. (2019). Exfoliated graphene-manganese oxide nanocomposite electrode materials for supercapacitor. Journal of Alloys and Compounds,770.

63- Wu, Y., Liu, S., Wang, H., Wang, X., Zhang, X., & Jin, G. (2013). A novel solvothermal synthesis ofMn3O4/graphenecomposites for supercapacitors. Electrochimica Acta,90, 210-218. doi: 10.1016/j.electacta.2012.11.124

64- Ghasemi, S., Hosseini, S. R., & Boore-Talari, O. (2018). Sonochemical assisted synthesis MnO2/RGO nanohybrid as effective electrode material for supercapacitor. UltrasonicsSonochemistry,40,675685.doi:10.1016/j.ultsonch.2017.08.013

65- Dong, J., Lu, G., Wu, F., Xu, C., Kang, X., & Cheng, Z. (2018). Facile synthesis of a nitrogen-doped graphene flower-like MnO 2 nanocomposite and its application in supercapacitors. Applied Surface Science,427, 986-993. doi: 10.1016/j.apsusc.2017.07.291

66- Wang, H., Hu, Z., Chang, Y., Chen, Y., Zhang, Z., Yang, Y., & Wu, H. (2011). Preparation of reduced graphene oxide/cobalt oxide composites and their enhanced capacitive behaviours by homogeneous incorporation of reduced graphene oxide sheets in cobalt oxide matrix. Materials Chemistry and Physics,130(1-2), 672-679. doi: 10.1016/j.matchemphys.2011.07.043

67- Nguyen, T. T., Nguyen, V. H., Deivasigamani, R. K., Kharismadewi, D., Iwai, Y., & Shim, J. (2016). Facile synthesis of cobalt oxide/reduced graphene oxide composites for

electrochemical capacitor and sensor applications. Solid State Sciences,53, 71-77. doi: 10.1016/j.solidstatesciences.2016.01.006

68- Dong, X., Xu, H., Wang, X., Huang, Y., Chan-Park, M. B., Zhang, H., . . . Chen, P. (2012). 3D Graphene–Cobalt Oxide Electrode for High-Performance Supercapacitor and Enzymeless Glucose Detection. ACS Nano,6(4), 3206-3213. doi:10.1021/nn300097q

69- Naveen, A. N., Manimaran, P., & Selladurai, S. (2015). Cobalt oxide (Co3O4)/graphene nanosheets (GNS) composite prepared by novel route for supercapacitor application. Journal of Materials Science: Materials in Electronics,26(11), 8988-9000. doi:10.1007/s10854-015-3582-2

70- Xing, Z., Chu, Q., Ren, X., Tian, J., Asiri, A. M., Alamry, K. A., . . . Sun, X. (2013). Biomolecule-assisted synthesis of nickel sulfides/reduced graphene oxide nanocomposites as electrode materials for supercapacitors. Electrochemistry Communications,32, 9-13. doi: 10.1016/j.elecom.2013.03.033

71- Huang, K., Zhang, J., Liu, Y., & Liu, Y. (2015). Synthesis of reduced graphene oxide wrapped-copper sulfide hollow spheres as electrode material for supercapacitor. International Journal of Hydrogen Energy,40(32), 10158-10167. doi: 10.1016/j.ijhydene.2015.05.152

72- Ramachandran, R., Saranya, M., Kollu, P., Raghupathy, B. P., Jeong, S. K., & Grace, A. N. (2015). Solvothermal synthesis of Zinc sulfide decorated Graphene (ZnS/G) nanocomposites for novel Supercapacitor electrodes. Electrochimica Acta,178, 647-657. doi: 10.1016/j.electacta.2015.08.010

73- Ratha, S., & Rout, C. S. (2013). Supercapacitor Electrodes Based on Layered Tungsten Disulfide-Reduced Graphene Oxide Hybrids Synthesized by a Facile Hydrothermal Method. ACS Applied Materials & Interfaces,5(21), 11427-11433. doi:10.1021/am403663f

74- Supercapacitor Electrodes Obtained by Directly Bonding 2D MoS 2 on Reduced Graphene Oxide

75- Cai, W., Lai, T., Lai, J., Xie, H., Ouyang, L., Ye, J., & Yu, C. (2016). Transition metal sulfides grown on graphene fibers for wearable asymmetric supercapacitors with high

volumetric capacitance and high energy density. Scientific Reports,6(1). doi:10.1038/srep26890

76- Meng, X., Deng, J., Zhu, J., Bi, H., Kan, E., & Wang, X. (2016). Cobalt Sulfide/Graphene Composite Hydrogel as Electrode for High-Performance Pseudocapacitors. Scientific Reports,6(1). doi:10.1038/srep21717

77- Xu, L., & Lu, Y. (2015). One-step synthesis of a cobalt sulfide/reduced graphene oxide composite used as an electrode material for supercapacitors. RSC Advances,5(83), 67518-67523. doi:10.1039/c5ra11711a

78- Kim, J., Kim, K., Kim, H., Park, S., Roh, K. C., & Kim, K. (2015). Template-Free Synthesis of Ruthenium Oxide Nanotubes for High-Performance Electrochemical Capacitors. ACS Applied Materials & Interfaces,7(30), 16686-16693. doi:10.1021/acsami.5b04360

79- Sarkar, A., Satpati, A. K., Kumar, V., & Kumar, S. (2015). Sol-gel synthesis of manganese oxide films and their predominant electrochemical properties. Electrochimica Acta,167, 126-131. doi: 10.1016/j.electacta.2015.03.172

80- Pei, L., Zhang, X., Zhang, L., Zhang, Y., & Xu, Y. (2016). Solvent influence on the morphology and supercapacitor performance of the nickel oxide. Materials Letters,162, 238-241. doi: 10.1016/j.matlet.2015.10.029

81- Kandalkar, S., Gunjakar, J., & Lokhande, C. (2008). Preparation of cobalt oxide thin films and its use in supercapacitor application. Applied Surface Science,254(17), 5540-5544. doi: 10.1016/j.apsusc.2008.02.163

82- Xu, J., Gao, L., Cao, J., Wang, W., & Chen, Z. (2010). Preparation and electrochemical capacitance of cobalt oxide (Co3O4) nanotubes as supercapacitor material. Electrochimica Acta,56(2), 732-736. doi: 10.1016/j.electacta.2010.09.092

83- Chen, W., Xia, C., & Alshareef, H. N. (2014). One-Step Electrodeposited Nickel Cobalt Sulfide Nanosheet Arrays for High-Performance Asymmetric Supercapacitors. ACS Nano,8(9), 9531-9541. doi:10.1021/nn503814y

84- Yang, J., Duan, X., Qin, Q., & Zheng, W. (2013). Solvothermal synthesis of hierarchical flower-like β-NiS with excellent electrochemical performance for supercapacitors. Journal of Materials Chemistry A,1(27), 7880. doi:10.1039/c3ta11167a

85- Krishnamoorthy, K., Pazhamalai, P., & Kim, S. J. (2017). Ruthenium sulfide nanoparticles as a new pseudocapacitive material for supercapacitor. Electrochimica Acta,227, 85-94. doi: 10.1016/j.electacta.2016.12.171

86- Zhu, T., Xia, B., Zhou, L., & Lou, X. W. (2012). Arrays of ultrafine CuS nanoneedles supported on a CNT backbone for application in supercapacitors. Journal of Materials Chemistry,22(16), 7851. doi:10.1039/c2jm30437f

87- Yang, Z., Chen, C., & Chang, H. (2011). Supercapacitors incorporating hollow cobalt sulfide hexagonal nanosheets. Journal of Power Sources,196(18), 7874-7877. doi: 10.1016/j.jpowsour.2011.03.072

Chapter Four: Materials and Methods

4.1 Materials

Graphitic powder (size < 20 μm), nickel foam, Sodium Nitrate ($NaNO_3$, 99.9%), Cobalt chloride ($CoCl_2$, 99.9%) and polyvinylidene difluoride (PVDF) were all purchased from Sigma Aldrich. Hydrogen Chloride (HCL, 33%) and absolute ethanol are purchased from El-Nasr Pharmaceutical Company in Egypt Whilst Absolute Sulfuric acid (H_2SO_4, 99%) was purchased from Sham Lab.30 % W/ V Hydrogen peroxide from LOBA Chemie. In addition, potassium permanganate ($KMnO_4$, 99%) from the Arabic Laboratory Equipment Company. Finally, Adenine and sulphanilamide were purchased from Merk. For washing and dispersing the products, Distilled water and Deionized water were used .

4.2 Synthesis methods

4.2.1 **spongy graphene oxide fabrication (SGO)**

Modified Hummers' method was employed to prepare GO. (1). In such approach, (1.5 g) of graphite, (1.5 g) of $NaNO_3$ and (70 ml) of H_2SO_4 were mixed together followed by stirring in an ice bath. The above-mentioned procedure was then followed by the addition of 9 g of $KMnO_4$. The formed mixture was heated to 40◦C and stirred for an hour. 100 ml of distilled water was added and the whole reaction mixture was heated for 30 mins at 90°C. This was finally followed by the addition of 300 ml of distilled water slowly. 10 ml of 30% H_2O_2 was added subsequently. Filtration and washing were done by the aid of HCl(0.1 M) and distilled water. The formed GO precipitate underwent three centrifugation steps at 10000 rpm for 30 min in order to get purified. This step was performed after having been dispersed in a water/methanol (1:5) blend. Dispersion of the pure samples was carried out in deionized water followed by centrifuging at 2500 rpm. This was followed by step sonicating the dispersed GO for 1 hour to obtain exfoliated graphene oxide. The last step involved dispersion of GO precipitate in water/methanol mixture and purification with repeated centrifugation steps at 10000 rpm for 30 min. Regarding preparing spongy graphene oxide(SGO), (5 mg/l) of GO were put in a freeze rat a low temperature of -18 C for 2 consecutive days. This was followed by the transfer of frozen GO tubes into a freeze-dryer at a very low temperature of -53 °C and a pressure of 10 Pa for 3 days. (2). see fig.4.1.

4.2.2 Adenine-functionalized graphene oxide synthesis

0.1g of the freeze-dried GO was dispersed in 10 ml of distilled water. Then an equimolar amount of NaOH and 0.3 g of adenine were mixed together in 10 ml of distilled water. The afore mentioned and the later mixtures added to each other. They product mixture was then stirred for 24 h . Centrifuging was done, and the mixture was washed several times with water and ethanol mixtures Finally, the product was dries at 60 °C., see fig. 4.1.

4.2.3 Preparation of CoS and functionalized graphene (FG-COS) Powder

Cobalt sulfide was prepared using hydrothermal reduction method. In such method, 25 mg of cobalt chloride ($CoCl_2$) and 50 mg of sulfanilamide were added to a 100ml flask. This was followed by the addition of c40ml of deionized water. To obtain homogeneous dispersion, sonication was carried out for 30 min. As for the hydrothermal reduction, the solution was transferred to a Teflon-lined autoclave and heated at 170 °C for 24h. The solution was then left to cool room temperature. This was followed by washing the product with deionized water several times. Finally, CoS was dried in an oven at 60 °C. Preparation of functionalized graphene–Cobalt Sulfide (FG-CoS): The functionalized graphene–CoS by using sulfanilamide (FG-CoS-SA). Briefly a specific amount of functionalized graphene oxide powder was dispersed in 20 ml DI water and sonicated for 1 h (4). Later, cobalt chloride equivalent to 30 wt. % from FGO mass and 0.2g of sulphanilamide were added to the above suspension under sonication for 35 min to obtain a homogeneous dispersion; The solutions were transferred to a Teflon-lined autoclaves and heated at 170 °C for 24h, and were left to cool at room temperature. This was followed by washing the products several times with deionized water and collected through centrifugation. Finally, the solid products were dried in an oven at 60 °C. The steps are summarized in Fig.4.1.

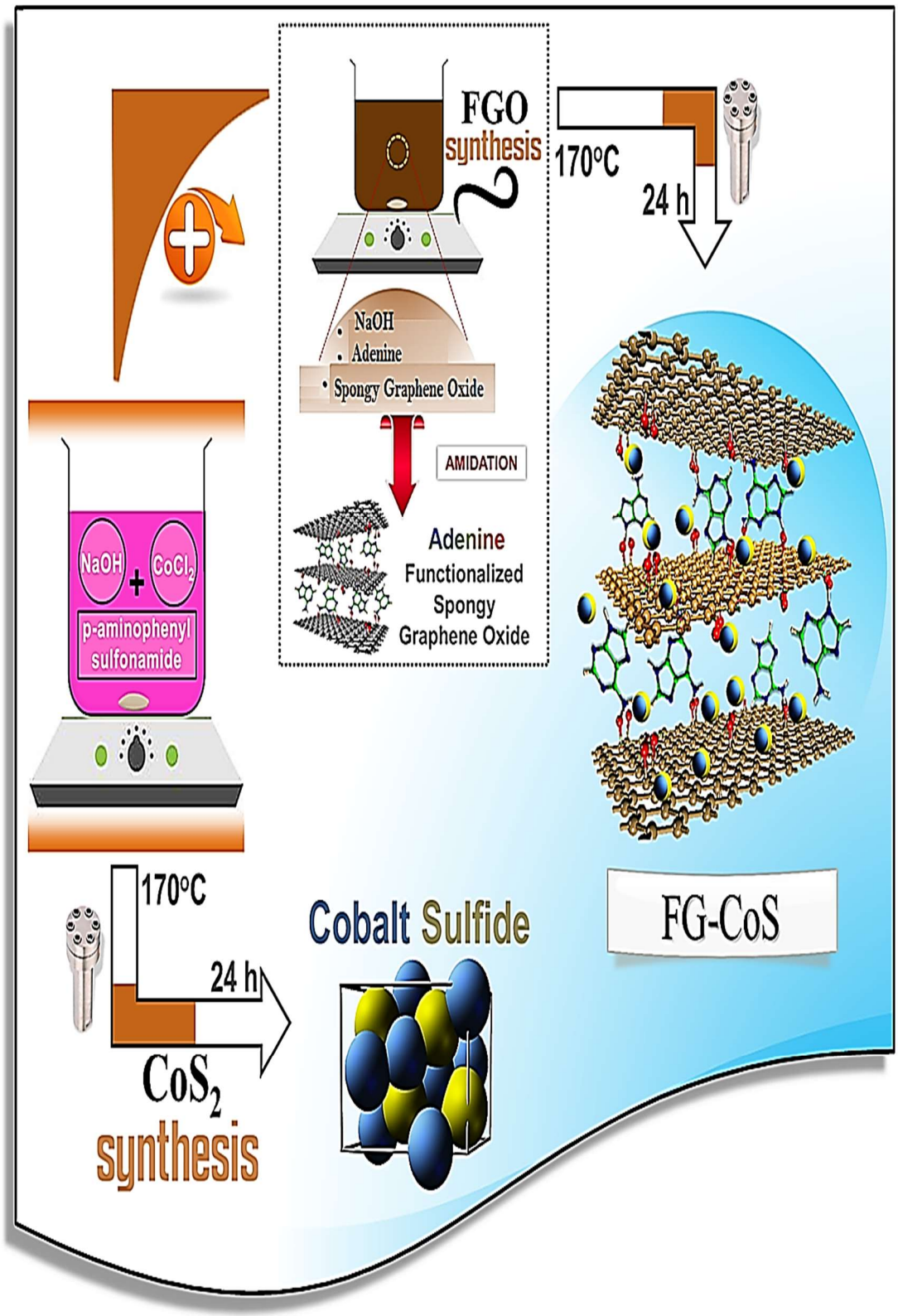

Fig 4.1: Scheme of Synthesis of CoS and FG-CoS

4.2.4 Preparation of electrodes and electrochemical measurements

An electrode was fabricated by mixing 90 wt. % of FG-CoS, and 10 wt. % of poly vinylidene di fluoride in N-methyl-2-pyrrolidinone. The working electrode is made from Ni foil, which was is cleaned via ultrasonication in ethanol and acetone for 10 minutes each then dried Then, the slurry was applied to the polished Ni foil using a micro pipette (area of coating: 1 cm^2, and foil thickness: 0.2 mm).In order to proceed with characterization, the working electrode was dried at 60 °C for 24 h. All the electrochemical measurements were performed in a three-electrode system. The working electrode is Ni foil, the standard being calomel electrode (SCE) and platinum wire were used as counter. The electrolyte used is 3 M KOH. Electrochemical measurements were performed using using CHI electrochemical workstation. Cyclic voltammetry (CV) measurements were done in the potential range 0 to 0.5 V at various scan rates (1-100 mV/s). Galvanostatic charge/discharge measurements were run in the potential range 0 to 0.5 V at current densities of 1, 2, 3, and 4 A/g respectively. The difference in mass between the initial, and impregnated nickel foil is taken to be the active mass of the electrode.

4.3 Characterization techniques

X-ray diffraction was measured by the diffractometer (XRD, XPERT- PRO- Analytical) with Cu Kα radiation (λ = 1.54 ºA) to examine crystal structure of the prepared materials. Surface morphology was examined by field-emission scanning electron microscope (FESEM-Zeiss SEM Ultra-60). The infrared (IR) spectra were measured using a JASCO spectrometer (FT/IR-6300 type A) in the range 400-4000 cm-1, and finally, Raman measurements for exploring chemical structure were performed using a micro-Raman microscope with an excitation laser beam wavelength of 325 nm.

4.3.1 Physical Characterization

4.3.1.1 Crystallinity

As mentioned, the crystal structure of the prepared materials was examined by X-ray diffraction (XRD, XPERT- PRO- Analytical) with Cu Kα radiation (λ = 1.54 °A). XRD is an analytical technique used to identify spacing of planes and hence structure of a

crystalline material through its unique diffraction pattern. X-ray diffraction is based on the principle of constructive interference between the incident x-rays and the target crystal sample. Constructive interference occurs only when Bragg's rule is satisfied $n\lambda=2d$ sin where λ is the wavelength of the incident x-ray radiation, d is the inter- planer spacing and θ is the diffraction angle. The diffracted X-rays are then detected hence counted. By scanning the sample through a range of 2θ angles, all possible diffraction patterns of the lattice should be deduced. Conversion of the diffraction peaks to d-spacings makes identification of the mineral possible, since each mineral has a set of unique d-spacings. Then by comparing the d-spacing to a reference pattern the material of interest can be identified. (5).

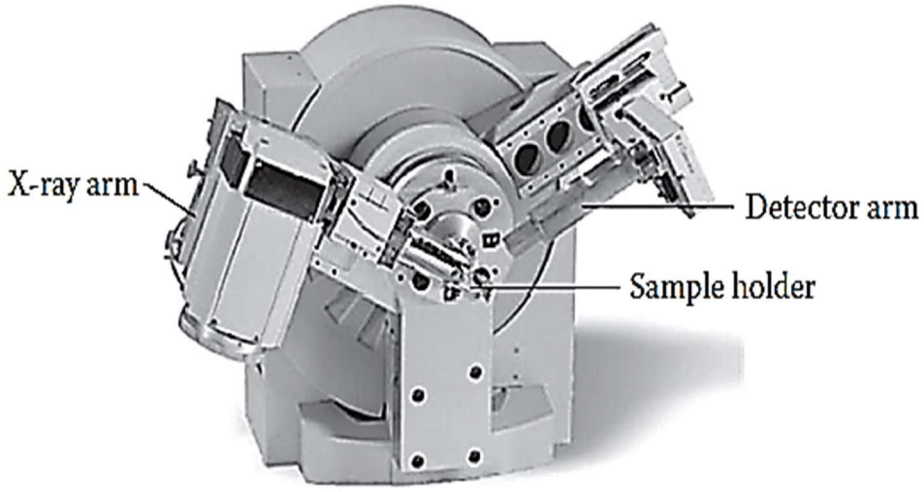

Fig 4.2:Modern X-ray diffractometer. (Courtesy of Panalytics, XPert Powder) (5)

Diffraction pattern of graphite appeared at 2Θ = 26.5°. The spectra of graphite oxide (GO) showed a sharp and lone diffraction peak at 2Θ = 12°. In addition to this, there appears a broad diffraction peak at 2Θ of 24.7°.

4.3.1.2 Morphology

Field-emission scanning electron microscope (FESEM-Zeiss SEM Ultra-60) was used to investigate surface morphology by at AUC. Powder samples of FG, FG-CoS, and CoS were gold coated (to increase conductivity) and placed on the sample stub. A Scanning Electron Microscopy uses a collimated high energy electron beam of very low wavelength to collect a highly magnified image of the target samples' topography. SEM provides information

about the material's surface morphology. Due to the very high resolution of SEM, it can determine the pore size of a nanotube. (6)

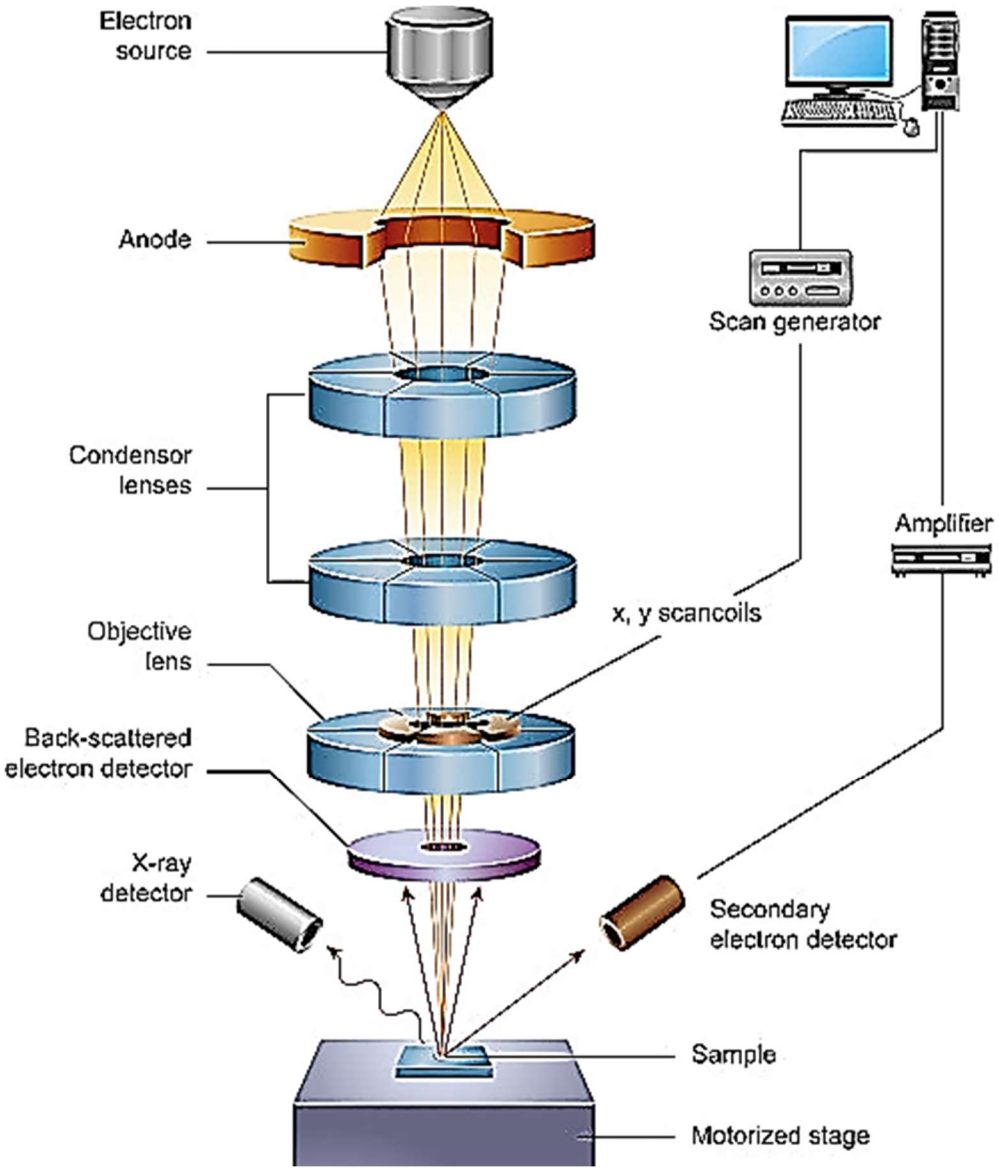

Fig 4.3:Materials Characterization Using Non-destructive Evaluation (NDE) Methods (7)

4.3.1.3 Composition

Raman spectroscopy is a spectrometric technique used to identify different modes of vibrations of molecules through the intensity of scattered light beam (8). The molecules absorb the incident photons, they get excited, and then re-emit photons of different wavelengths, returning the molecule to a different rotational or vibrational state than its original ground state. This difference in energy is detected in the form of wavelength shift. Raman spectroscopy gives insight about the molecules' functional group, which in turns defines chemical reactivity and all chemical properties of a given molecule. (9). A micro-Raman microscope with an excitation laser beam wavelength of 325 nm was used to examine chemical structure .

Moreover, infrared (IR) spectra were recorded using a JASCO spectrometer (FT/IR-6300 type A) in the range 400-4000 cm-1 to determine functional groups present. In addition, EDX analysis spectrum (FG-COS) was carried to study the compositions' elements.

4.3.2 Electrochemical Characterization

4.3.2.1 Cyclic Voltammetry

Cyclic voltammetry is an electrochemical transient technique used to investigate the electrochemical behaviour of a system. In this process the electrode is being subject to a voltage sweep between two fixed values. The CV scan is a plot of the current passing between the working electrode and counter electrode verses potential which determines the potential at which redox process occur. This current normalized by the electrode surface area is referred to as current density. (10). The plot of current density vs. scan potential is called a voltammogram. Specific capacitance is measured using

$$Cs = \frac{\int Idv}{vm\Delta V} \qquad (4.1)$$

where Cs is the specific capacitance of the prepared electrode, m is the weight of the electrode material (g), I is the response current density (A/g), ΔV is the potential difference, and v is the potential scan rate (mV/s). Cyclic voltammetry was carried at a scan rate of 1, 5, 10, 25, 50, and 100 mv.

4.3.2.2 Galvanostatic charge/discharge

Galvanostatic cycling (chronopotentiometry), is an electrochemical characterization technique, which can give an insight about capacitance, resistance and cyclability. In this technique, current is controlled, and voltage is fixed. (11). The specific capacitance is calculated at various current densities using the following equation:

$$Cs = \frac{\int \mathrm{I}\,\Delta \mathrm{t}}{\mathrm{m}\,\Delta \mathrm{V}} \qquad (4.2)$$

I is the discharge current (A), Δt is the discharge time (s), and ΔV is the potential window (V).Values of specific capacitance were calculated at current densities of 1, 2, 4, and 5 A/g.

4.3.3.3 Cycle life measurement using Charging-Discharging curves

Charging-Discharging over many cycles, is an efficient way to study a supercapacitor's degradation. This enables to calculate specific capacitance values to determine retention or degradation of the supercapacitor. Our case showed a capacitance retention even after the 100^{th} cycle.

References:

1- Hummer, W. S. (1958). Preparation of Graphitic Oxide. *J. Am. Chem. Soc.,80*.

2- Xu, X., Pan, L., Liu, Y., Lu, T., Sun, Z., & Chua, D. H. (2015). Facile synthesis of novel graphene sponge for high performance capacitive deionization. *Scientific Reports,5*(1). doi:10.1038/srep08458

3- Mallakpour, S., Abdolmaleki, A., & Borandeh, S. (2014). Covalently functionalized graphene sheets with biocompatible natural amino acids. *Applied Surface Science,307*, 533-542. doi: 10.1016/j.apsusc.2014.04.070

4- Dinh, D. A. (n.d.). Graphene: Three-Dimensional Graphene—A Prospective Architecture for High-Performance Supercapacitors. *CRC Concise Encyclopedia of Nanotechnology,*282-308. doi:10.1201/b19457-27

5- X-ray Powder Diffraction (XRD). (2019, March 05). Retrieved from https://serc.carleton.edu/research_education/geochemsheets/techniques/XRD.html

6- Spiegelberg, S., Kozak, A., & Braithwaite, G. (2016). Characterization of Physical, Chemical, and Mechanical Properties of UHMWPE. *UHMWPE Biomaterials Handbook,*531-552. doi:10.1016/b978-0-323-35401-1.00029-6

7- Materials Characterization Using Non-destructive Evaluation (NDE) Methods. (2016). doi:10.1016/c2014-0-00661-2

8- Introduction to Raman Spectroscopy - B&W Tek. (n.d.). Retrieved from http://bwtek.com/raman-introduction-to-raman-spectroscopy/

9- Practical Raman Spectroscopy | SpringerLink. (n.d.). Retrieved from https://link.springer.com/book/10.1007/978-3-642-74040-4

10- Elgrishi, N., Rountree, K. J., Mccarthy, B. D., Rountree, E. S., Eisenhart, T. T., & Dempsey, J. L. (2017). A Practical Beginner's Guide to Cyclic Voltammetry. *Journal of Chemical Education,95*(2), 197-206. doi: 10.1021/acs.jchemed.7b00361

11- Nickel-based materials for supercapacitors. (2018, December 21). Retrieved from https://www.sciencedirect.com/science/article/pii/S136970211830624

Chapter Five: Results and discussion:

Herein, we demonstrate a facile and green method to prepare spongy functionalized graphene/CoS (FG-CoS) composite electrodes for supercapacitor applications. A simple approach is illustrated to synthesize functionalized spongy graphene/cobalt sulfide (FG-CoS) nanocomposites as interconnected, porous 3-dimensional (3D) network crinkly sheets which contain the reduction of SGO sheets and intercalated of CoS nanoparticles with spongy graphene. The formed special 3D structure provides this composite through high electrochemical performance. Physical Characterization of the fabricated FG-CoS was by X-ray diffraction (XRD), scanning electron microscopy (FESEM) and Raman spectroscopy. Whilst electrochemical characterization was performed in 3M KOH using cyclic voltammetry (CV)in a potential window from 0-0.5 V at different potential scan rates. Galvanostatic charge/discharge was performed at current densities of 1,2,3, and 5 A/g respectively..

5.1 Physical Characterization

5.1.1 Surface morphology (FESEM)

Figure 5.1 shows FESEM images and EDX spectra of the synthesized materials. Figure 1a describes the surface of the fabricated spongy graphene oxide (SGO). The large thickness of the layers is possibly due to the formation of oxygen -containing groups in the basal plane of graphene. Figure 5.1b depicts the morphology of the CoS synthesized with sulphanilamide with the inset showing a junk of nanoparticles with very fine particle size. Figure 5.1c shows the morphology of the fabricated SG/CoS composite, where graphene sheets become more exfoliated, exhibiting an interconnected, porous 3D framework of randomly oriented, and crinkly sheets. Those wrinkles can act to prevent graphene sheets from restacking. Not only the uniformly distributed CoS but also the sulphanilamide played an important role in preventing the restacking of the sheets. Moreover, the existence of sulphanilamide effectively restrains the agglomeration of fine nanoparticles with high energy. This is favourable for the formation of CoS nanocrystals. Afterwards, the formed nucleus gradually grew into hexagonal-like nanoparticles and *in-situ* deposited on both sides of graphene sheets. At the same time,

FGO was reduced during the hydrothermal process and self-assembled to form the final composite hydrogel (FG-CoS) with cross-linked 3D network, owing to π-π stacking interaction of conjugated FG sheets. Figure 5.1d shows the EDX spectrum of FG-CoS, which confirms the presence of Co, S, and C in the FG/CoS nanocomposite with the inset showing the weight % of the detected elements.

FG sheets. EDX analysis spectrum (FG-COS) shown in Fig.5.4, Shows the EDX spectrum, which confirms the presence of CoS in the FG/CoS nanocomposite.

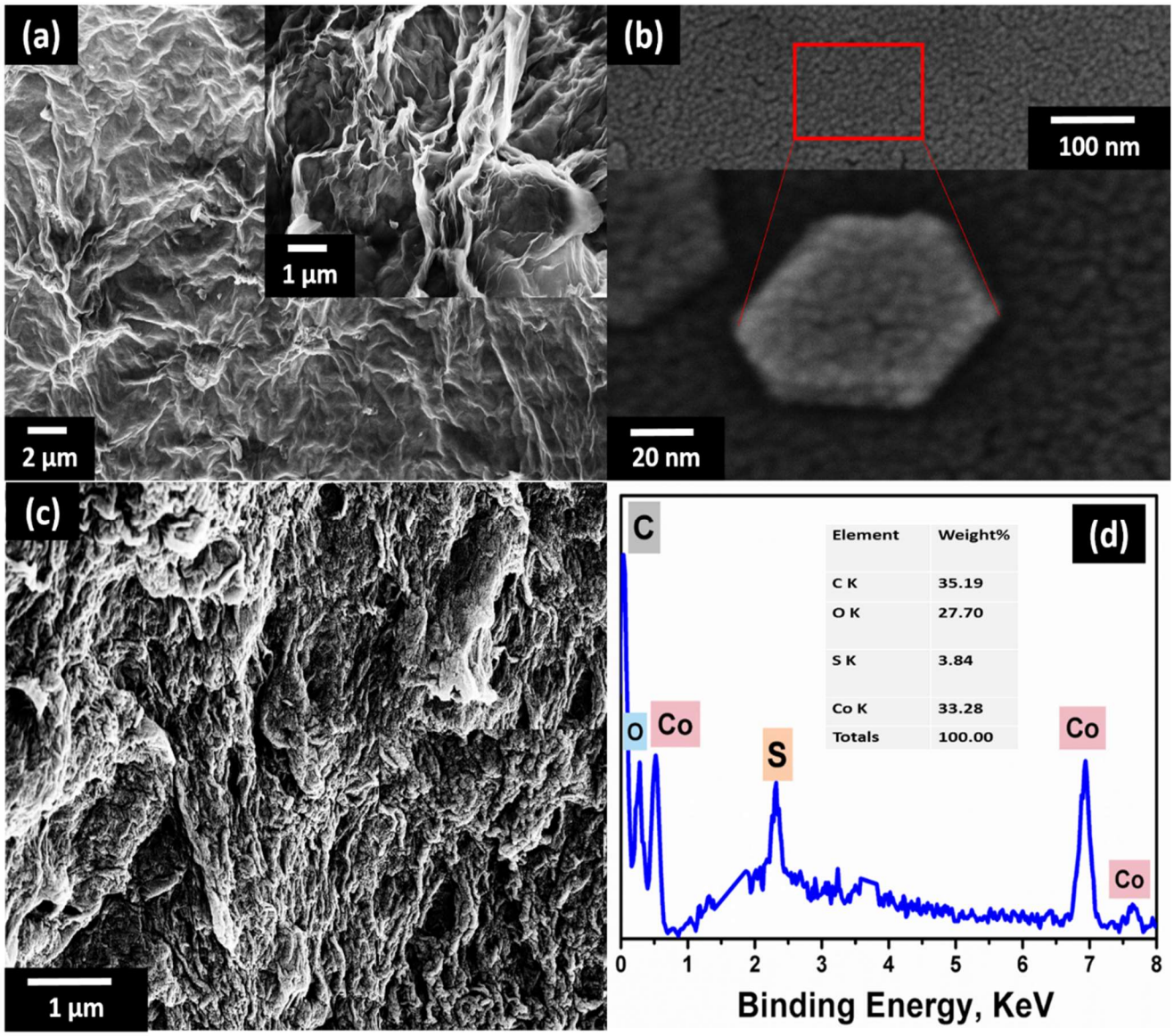

Figure 5.1: FESEM images of (a) spongy graphene oxide (SGO), (b) CoS, (c) FG-CoS, and (d) EDX spectra of the FG-CoS nanocomposite.

5.1.2 Crystallinity, composition and chemical structure.

Figure 5.2a shows the XRD pattern of bare graphite, SGO, FGO, CoS, and FG-CoS. The lone sharp peak which appeared in the diffraction pattern of graphite at 2Θ = 26.5° corresponds to interlayer spacing of 0.34 nm and reflection from the (0 0 2) plane. The spectra of graphite oxide (GO) shows a single and sharp diffraction peak at 2Θ = 12°this corresponds to an interlayer spacing of 0.83 nm, suggesting no remaining native graphite (1). The increase in the d-value of GO (from 0.34 to 0.83 nm) is due to the increase in the interlayer spacing along the c-axis. This can be related to the presence of oxygen atoms as a result of rapid oxidation of the GO sheets (2), confirming that SGO is converted into FGO after functionalization. Upon reducing the FGO with cobalt chloride, there appears a broad diffraction peak at 2Θ of 24.7°. Moreover, the in-situ formed CoS nanoparticles might attach onto FG sheets during the hydrothermal treatment, preventing their aggregation and restacking, which also could weaken the peak intensity of FG-CoS. Compared with the pattern of bare CoS, the peaks at 30.7°, 36.0°, 47.5°, and 54.2° are attributed to [100], [101], [102], and [110] faces of CoS (JCPDS No. 65-3418, hexagonal phase) becoming weaker in intensity and broader in width. This may imply that the composite has a lower crystallinity due to the existence of the CoS impurity, which is confirmed by EDX analysis spectrum of FG-CoS shown in Fig. 5.1d (3). Figure 5.2b represents the FTIR spectra of GO, FGO, and FG-CoS. Various peeks appearing in the the FTIR spectrum corresponds to the presence of many functional groups. There appears band at about 1725 cm^{-1} can be credited to the stretching vibrations ν(C=O) of COOH group of carbonyl and carboxyl groups. Another band appearing at 1621 cm^{-1} which can be linked to the in-plane vibration (C=C) from un-oxidized sp^2 CC bonds. There is a broad band centred around 3563 cm^{-1} which might be associated to O-H stretching vibrations ν(OH_2) .This functional group can be related to adsorbed water. A sharp band at 1378 cm^{-1} can be linked to to O-H deformation of C–OH group. The recognized band at 1101 cm^{-1} is due to the ν(C–O) stretching vibrations mode (4). As for FGO,the peak at 1725 cm^{-1} almost disappears and another peak arisen at 1637 cm^{-1} which is characteristic of the C= O stretching in the amide group. A strong peak at 1188 cm^{-1} appeared due to the amide C-N bond stretching of the amide group . Other peaks at 1560 and 1618 cm^{-1} are related to the graphene vibration, The peak at 3415 cm^{-1} is specific for N−H stretching (5).Peaks corresponding to the OH and NH stretching groups appeared at 3475 cm^{-1} .These peaks confirm the covalent functionalization

of the graphite by adenine, hence indicating the simultaneous successful functionalization and reduction process .. These results assure that adenine molecules were covalently bonded to GO via amide group linkage. Note that the peak intensity of the C-O and C-O-C (epoxide) groups, respectively, was decreased in FGO and after the hydrothermal reduction that resulted in FG-CoS. On the contrary, the peak intensity of OH and carboxyl ions around 3000–3700 cm^{-1} was negligible in the FG-CoS nanocomposite, which can be attributed to the interaction between CoS and carboxyl groups. Note also that the interaction between the CoS and FG is very strong that they remained attached to the surface even after washing and strong sonication (6). Raman is used to investigate the crystal structure and the defect level of graphene and carbon-based materials. Figure 5.2c shows the Raman spectra of GO and compared to that of FG-CoS. Two main peaks were observed that are located at approximately 1350 and 1590 cm^{-1}, corresponding to D-band and G-band. The intensity ratio of the D and G bands (I_D/I_G) is a useful parameter for determining degree of reduction of GO .It determines the portion of the present sp^2 and sp^3 . (7). The higher I_D/I_G ratio of FG-CoS (1.04) than that of GO (0.98) is attributed to the intercalated CoS nanoparticles with FG during the formation of the composite, which is in agreement with the XRD results.

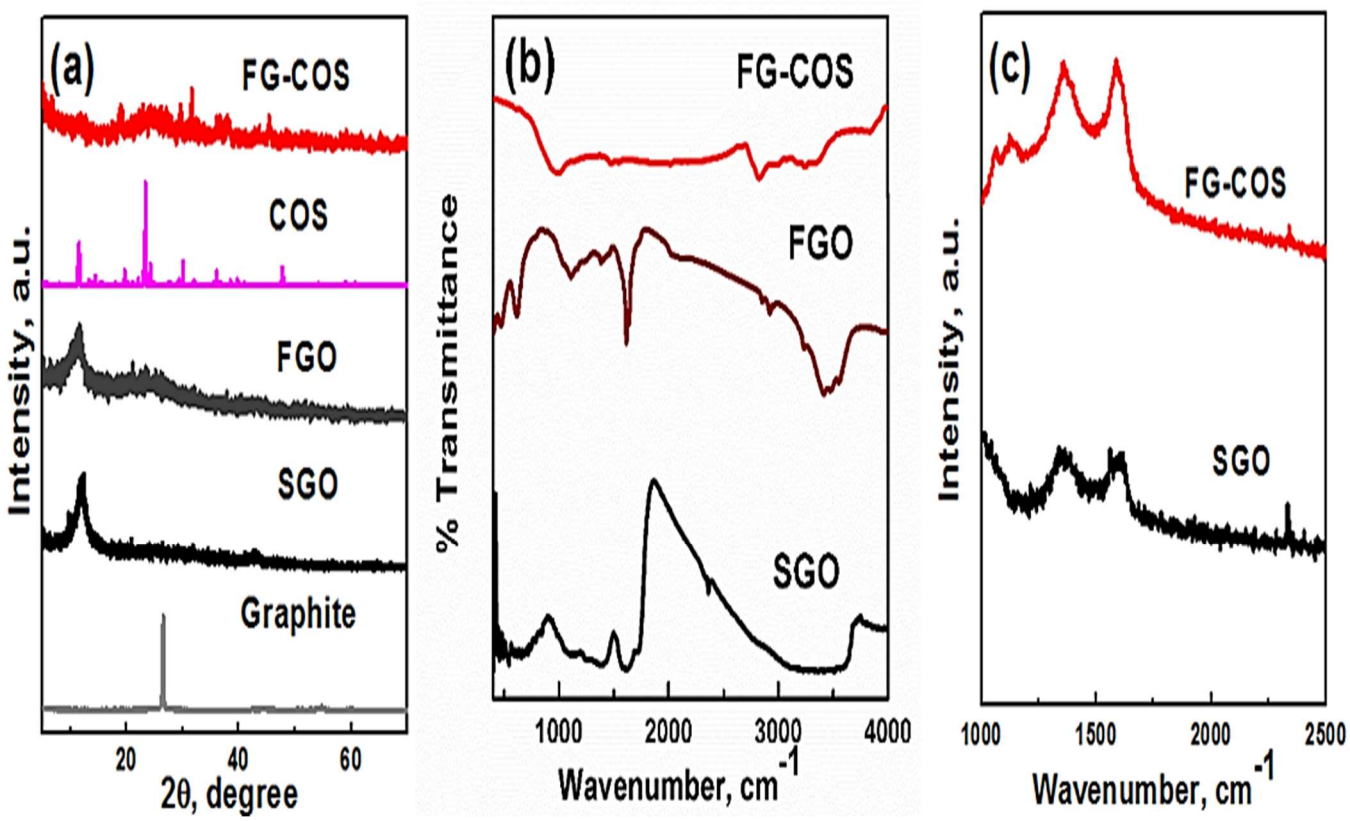

Fig. 5.2. (a) XRD pattern, (b) FTIR spectra, and (c) Raman spectra of the fabricated materials

5.2 Electrochemical Characterization

5.2.1 Cyclic Voltammetry measurements

To Study supercapacitive behaviour of the synthesized electrodes, cyclic voltammetry (CV) measurements were performed in 3M KOH, and the specific capacitance of the electrodes was calculated using Eq. 5.1.

$$Cs = \frac{\int Idv}{vm\Delta V} \qquad (5.1)$$

Cs is being is the specific capacitance, *m* is the weight of the electrode material (g), *I* is the response current density (A/g), ΔV is the potential difference, and v is the potential scan rate (mV/s). Figure 5.3a represents the cyclic voltammograms of the FG-CoS and SGO electrodes in 3M KOH aqueous electrolyte at 1 mV/s scan rate. The SGO electrode shows negligible current response due to its insulating characteristics, the current of the FG-CoS electrode increases as the potential increases. This behaviour can be ascribed to the faradaic and non-faradaic reactions arising from graphene and cobalt sulfide CoS in the FG-CoS electrode. Figure 5.3b demonstrates that the specific capacitance of the FG-CoS electrode can reach 1072 F/g at a scan rate of 1 mV/s. Specific capacitance value dropped to 237 F/g at a scan rate of 100 mV/s as shown in Fig.5.3c. The reason for this decline in specific capacitance value at high scan rates is due to the diffusion limitation on the electrolyte ions, as they are not given enough time to enter into the complex micro pores of the electrode. This high specific capacitance value of the FG-CoS could be attributed to the synergetic effect of the RGO and CoS. The anchored Cos nanoparticles to the surface of RGO induced porosity and hence increased the accessible surface area for electrolyte ions diffusion. This contributed in pseudo capacitance and the overall capacitance of the FG-CoS composite. The FG-CoS electrode showed much higher capacitance than that of CoS nanoparticles at different scan rates. The obtained specific capacitance of 1072 F/g at a scan rate of 1 mV/s is much higher than that previously reported for CoS_2–graphene nanocomposite prepared by solvothermal method (253 F/g in 6 M KOH solution at 5 mV/s) (8), indicating the superiority of our fabricated electrodes.

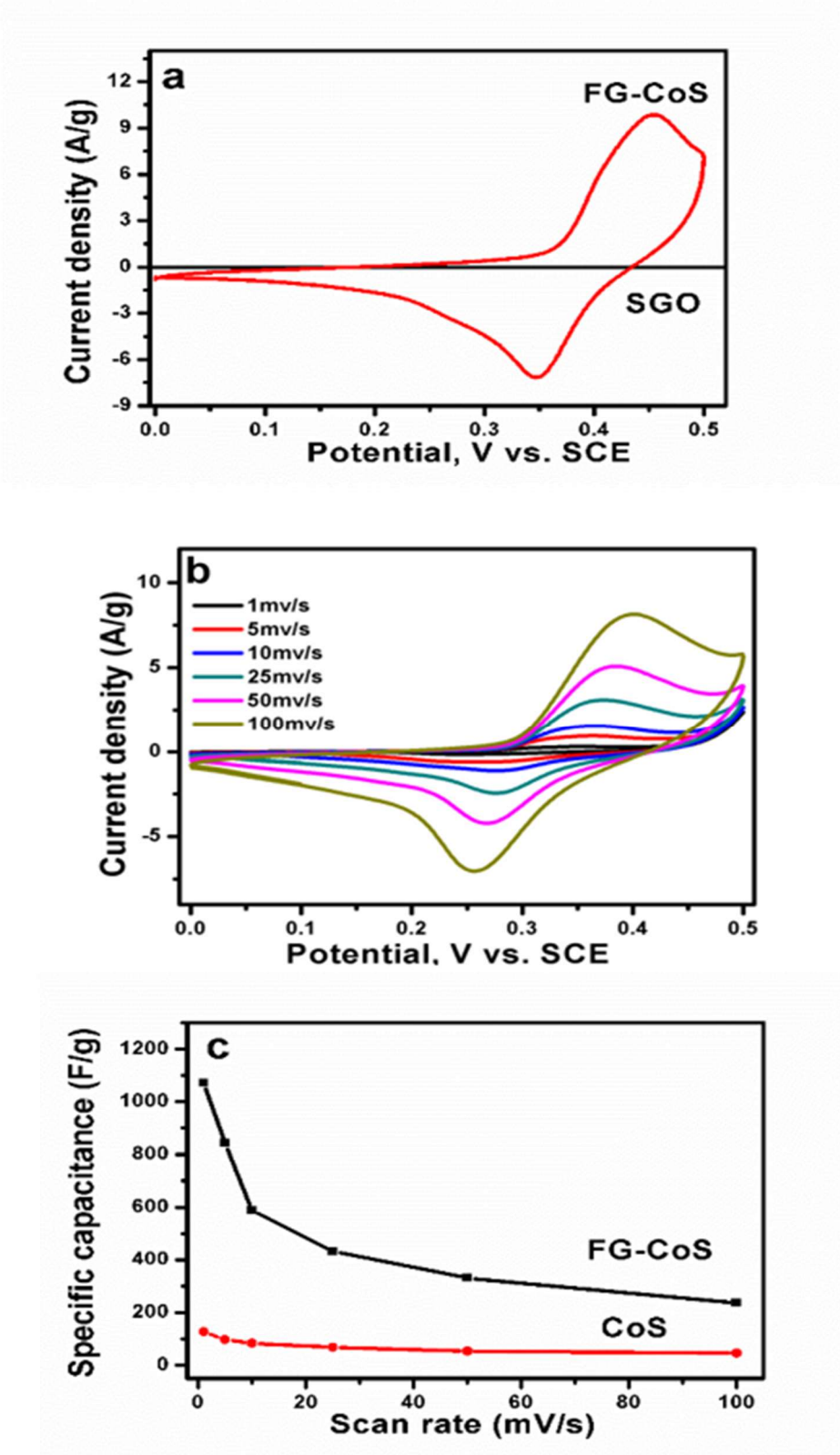

Fig. 5.3. (a) Cyclic voltammograms of FG-CoS and SGO electrodes in 3 M KOH at a scan rate of 5 mV/s, (b) cyclic voltammograms of FG-CoS electrodes at different scan rates, and (c) the corresponding specific capacitance of FG-CoS electrodes at different scan rates in 3 M KOH.

5.2.2 Galvanostatic charge/discharge

Galvanostatic charge/discharge measurement is essential to determine the performance of any material for use as a supercapacitor. Figure 5.4a reveals the galvanostatic charge/discharge graphs for the fabricated FG-CoS electrodes at different current densities (1, 2, 4, and 5 A/g). All the charge–discharge curves are quasi-triangular, indicating fast, capable charge transfer and the presence of capacitive faradic charge storage. In addition, the non-uniformity in the triangular curves can be attributed to IR drop on the electrode/electrolyte interface. (9). This can be related to the high electronegativity due to the presence of active nitrogen and sulfur atoms from adenine and sulphanilamide. Moreover, the presence of CoS on graphene surface may have created dipoles (10, 11), which attract charged species of adenine and electrolyte ions into the surface (12, 13). Nitrogen , Sulphur, and Oxygen atoms present had an inductive effect due to their σ-bonded structure, which in turns enhanced specific capacitance value resulting in reversible Faradic redox reactions (14).

Fig. 5.4b indicates a decline in specific capacitance as the current density increases. The specific capacitance was calculated at different current densities using Eq. 5.2

$$Cs = \frac{I\,\Delta t}{m\,\Delta V} \qquad (5.2)$$

where I is the discharge current (A), Δt is the discharge time (s), and ΔV is the potential window (V). The calculated specific capacitances were 1013.7, 664.8, 589.9, and 484.5 F/g at 1, 2, 4, and 5 A/g,. The specific capacitance at 1 A/g is found to be 1013.7F/g, which is very close to that calculated from the CV graphs (1270 F/g at scan rate 1 mV/s). This value is much higher than that previously reported for 3D CoS/graphene composite hydrogel (564 F/g at 1 A/g using 6 M KOH electrolyte) (8), solvothermally synthesized CoS_2/graphene nanocomposite (314 at 6 M KOH) (14) and cobalt sulfide/reduced graphene oxide (550 F/g at 1 A/g in 6 M of KOH) [36] and (20-25), see Table5.1. Fig.5.4c shows that the specific capacitance is sharply increased from the initial cycle until the 1000^{th} cycle to reach 117% of the initial cycle, indicating an excellent cycling stability and retention of the FG-CoS electrodes.

Table 5.1: Specific capacitances reported for doped graphene compared to current work.

Material	Synthetic approach	Specific capacitance	Ref.
CoS_2/graphene nanocomposite	Solvothermal processing	314F/g in 6 M KOH	14
cobalt sulfide/rGO	Hydrothermal processing	550 F/g in 6 M of KOH	15
Graphene/TiO_2 hybrid	Microwave processing	165 F/g in 1 M Na_2SO_4	20
coating of TiO_2 on graphene	Atomic layer deposition	84 F/g in a 1 M KOH	21
sulfonated graphene/MnO_2/polyaniline	Polymerization reaction	276, 1 F/g in 1 M Na_2SO_4	22
$CoFe_2O_4$/rGO/polyaniline	Polymerization reaction	257 F/g in 1 M KOH	23
Graphene/MnO_2/Polyaniline	Polymerization reaction	380 F/g in 0.5 M Na_2SO_4	24
Graphene/MnO_2/polyaniline	Polymerization reaction	395 F/g in 1 M H_2SO_4	25
CoS_2/graphene nanocomposite	Solvothermal processing	253 F/g in 6 M KOH	26
Cobalt Sulfide/Functionalized Graphene	**Green, single-pot synthesis**	**1072 F/g in 3 M KOH**	**Current work**

5.2.3 Energy and power density

The energy and power densities are very important performance metrics of supercapacitors performance. In fact, the ultimate aim is to enhance the energy density capability of supercapacitors. Energy and power density can be depicted from the galvanostatic charge/discharge graphs using Eqs.5.3 and 5. 4.

$$E = \frac{1}{2}\, Cs(\Delta V)^2 = \frac{I\,\Delta V t}{2m} \tag{5.3}$$

$$P = \frac{E}{t} = \frac{I\,\Delta V}{m} \tag{5.4}$$

E and P refer to the mean energy density (Wh/Kg) and mean power density (W/Kg), Cs is the specific capacitance as obtained from the charge/discharge curves, *I* is the discharge current (A), *t* is the discharge time (h), ΔV is the potential window (V), and *m* is the mass of the FG-CoS electrode (kg). Ragone plot for the FG-CoS electrode at different current densities is shown in Fig. 5.4d. The energy density reaches to 35.2 Wh/Kg with a power density of 250 W/kg at 1.0 A/g. The energy and power density values of 16.82 Wh/Kg and 1250 W/Kg remain the same at a current density of 5 A/g. It is a necessity to state that the value of the obtained for FG-CoS electrode (35.2 Wh/Kg) is much higher than those reported for Cobalt sulfide/rGO(13.6) (15), thermally-reduced graphene (11.6 Wh/Kg) (16) and chemically-reduced graphene (11.5) Wh/Kg (17),

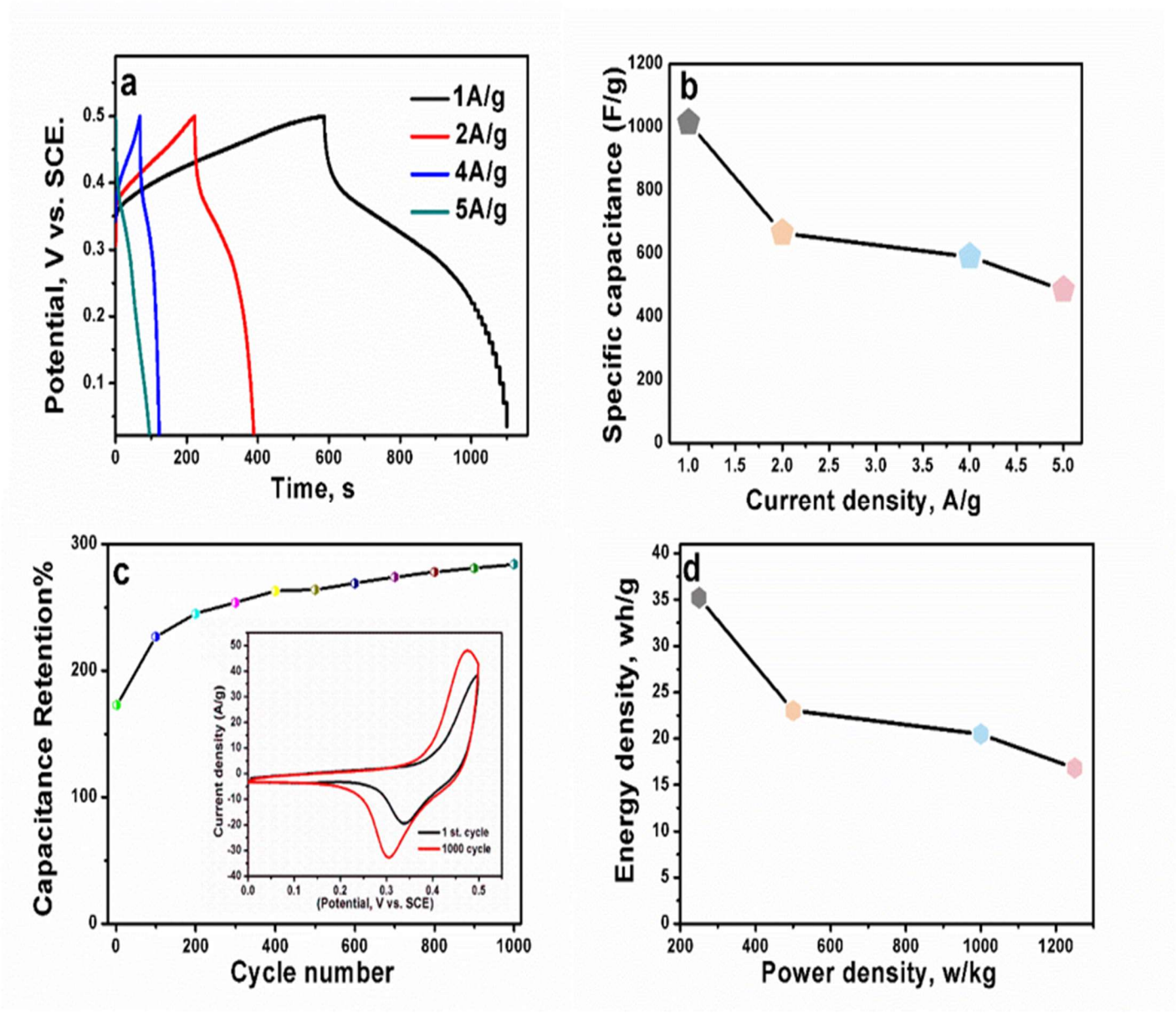

Fig. 5.4. (a) Galvanostatic charge/discharge, (b) variation of the specific capacitance with the current density, (c) the first and 1000thCV cycles of the FG-CoS electrodes, and (d) Ragone plot at different current densities of 1, 2, 4 and 5 A/g.

Table 5.2: Ragone table for reported energy and power density values compared to our work

Reference	**Material**	**Power density (W/Kg)**	**Energy density (Wh/Kg)**
15	Cobalt sulfide/rGO	1200	13.6
16	Graphene nanosheets	300	11.6
18	Carbon spheres/rGO	800	5.8
20	Graphene/TiO_2 hybrid	950	3.5
23	$CoFe_2O_4$/rGO/polyaniline	875	7.9
Current work	**Green, single-pot synthesis**	1250	16.82

References:

1. Xu Y, Bai H, Lu G, Li C, Shi G. Flexible Graphene Films via the Filtration of Water-Soluble Noncovalent Functionalized Graphene Sheets J. Am. Chem. Soc. 130 (2008) 5856.
2. Compton O C, Nguyen S T. Graphene oxide, highly reduced graphene oxide, and graphene: versatile building blocks for carbon-based materials. Small 6(6), 711–723 (2010).
3. Graupner R , Abraham J , Vencelová A , Seyller T , Hennrich F, Manfred M. Kappes, Hirschb A and Leya L . Doping of single-walled carbon nanotube bundles by Brønsted acids.Phys. Chem. Chem. Phys. 31, 13093–13100 (2013).
4. Zangmeister C D. Preparation and evaluation of graphite oxide reduced at 220 °C. Chem. Mater. (22), 5625 (2010).
5. Lei Z.,Lu L,Zhao XS .The electrocapacitive properties of graphene oxide reduced by urea. Energy Environ. Sci. (5), 6391 (2012).
6. Yang H, Li F, Shan C, Han D, Zhang Q , Niu L , Ivaska A . Covalent functionalization of chemically converted graphene sheets via silane and its reinforcement. J. Mater. Chem. (19), 4632–4638 (2009).
7. Hu H , Zhao Z , Zhou Q , Gogotsi Y , Qiu J. The role of microwave absorption on formation of graphene from graphite oxide .Carbon 50 (2012) 3267.
8. Ali B A, Metwalli O I, Khalil A S G, Allam N K. Unveiling the Effect of the Structure of Carbon Material on the Charge Storage Mechanism in MoS_2-Based Supercapacitors. ACS Omega 3 (2018) 16301−16308.
9. Shuai Z, Parvez K , Winter A , Vieker H , Liu X , Han S , Turchanin A , Feng X , üllen K. Layer-by-layer assembled hetero atom-doped graphene films with ultrahigh volumetric capacitance and rate capability for micro-supercapacitors. Adv. Mater. (26), 4552–4558 (2014).
10. Sun L, Tian C, Li M, Meng X, Wang L, Wang R, Yin J, Fu H. From coconut shell to porous graphene-like nano sheets for high-power super- capacitors. J. Mater. Chem. A (1), 6462–6470 (2013).
11. Hu J, Kang Z, Li F, Huang X. Graphene with three-dimensional architecture for high performance supercapacitor. Carbon (67), 221–229 (2014).

12. Wang H, Maiyalagan T, Wang X. Review on recent progress in nitrogen- doped graphene, Synthesis, characterization, and its potential applications, ACS Catal. (2), 781–794 (2012).
13. Chen C M, Zhang Q, Zhao X C, Zhang B, Kong Q, Yang M G, Yang Q H, Wang M Z, Yang Y G, Schlögl R, Su D S. Hierarchically aminated graphene honey combs for electro- chemical capacitive energy storage. J. Mater. Chem. (22), 14076–14084 (2012).
14. Meng X , Deng J , Zhu J , Bi H , Kan E & Wang X . Scientific Reports 6 (2016) 21717.
15. Xu L , Lu Y. One-step synthesis of a cobalt sulfide/reduced graphene oxide composite used as an electrode material for supercapacitors RSC Advances.,10 (2015).
16. C.M. Chen, Q.Zhang, M.G. Yang, C.H.Huang, Y.G.Yang, M.Z. Wang, Structural evolution during annealing of thermally reduced graphene nanosheets for application in supercapacitors. Carbon (50), 3572, (2012).
17. S.Y.Yang, K.H. Chang, H.W. Tien, Y.F. Lee, S.M. Li, Y .S. Wang, J.Y . Wang, C.C. M. Ma , C.C. Hu , Design and tailoring of a hierarchical graphene-carbon nanotube architecture for supercapacitors, J. Mater. Chem. (21), 2374 (2011).
18. Z. Lei, N. Christov, X. S. Zhao, Intercalation of mesoporous carbon spheres between reduced graphene oxide sheets for preparing high-rate supercapacitor electrodes. Energy Environ. Sci. (4), 1866 (2011).
19. Yang S Y , Chang K H , Tien H W , Lee Y F , Li S M , Wang Y S , Wang J Y , Ma C C M , Hu C C. Design and tailoring of a hierarchical graphene-carbon nanotube architecture for supercapacitors, J. Mater. Chem. (21), 2374 (2011).
20. Xiang C , Li M, Zhi M , Manivannan A , Wu N. Reduced graphene oxide/titanium dioxide composites for supercapacitor electrodes: shape and coupling effects. J Mater Chem. (22),19161–7(2012).
21. Sun X, Xie M, Wang G, Sun H , Cavanagh A S, J J, Steven T, George M , Liana J . Atomic Layer Deposition of TiO_2 on Graphene for Supercapacitors. Journal of The Electrochemical Society, (159), A364-A369 (2012).

22. Wang G , Tang Q, Bao H , Li X , Wang G. Synthesis of hierarchical sulfonated graphene/MnO2/polyaniline ternary composite and its improved electrochemical performance J Power Sources, 241 (2013), pp. 231-238.
23. Sankar V K , Selvan R. K .Fabrication of flexible fiber supercapacitor using covalently grafted $CoFe_2O4$/reduced graphene oxide/polyaniline and its electrochemical performances Electrochim Acta, 213 (2016), pp. 469-481
24. Yu G , Hu L, Liu N , Wang H , Vosgueritchian M , Yang Y .Enhancing the supercapacitor performance of graphene/MnO_2 nanostructured electrodes by conductive wrapping Nano Lett, 11 (2011), pp. 4438-4442.
25. Mu B , Zhang W , Shao S , Wang A .Glycol assisted synthesis of graphene-MnO_2-polyaniline ternary composites for high performance supercapacitor electrodes PCCP, 16 (2014), pp. 7872-7880
26. Wang, B., Park, J., Su, D., Wang, C., Ahn, H., & Wang, G. (2012). Solvothermal synthesis of CoS2–graphene nanocomposite material for high-performance supercapacitors. *Journal of Materials Chemistry,22*(31), 15750. doi:10.1039/c2jm31214j

Chapter six: Conclusion and future work

Conclusion

CoS-decorated 3-dimensional (3D) network crinkly sheets of functionalized spongy graphene (FG-CoS) nanocomposites were successfully synthesized via a simple and a green method. This provides better contact at the electrode/electrolyte interface and facilitates the charge transfer kinetics. The electron microscopy (FESEM) analysis showed the homogenous distribution of the CoS nanoparticles on the surface of the functionalized graphene sheets. EDX analysis spectrum confirms the presence of carbon, oxygen, sulfur, and cobalt. Also, the FTIR spectra showed a peak intensity of OH and carboxyl around 3000–3700 cm^{-1} was negligible in the FG-CoS nanocomposite, which can be attributed to the interaction between CoS and carboxyl groups. The higher I_D/I_G ratio of FG-CoS (1.04) than that of GO (0.98) is attributed to the intercalated CoS nanoparticles with FG. The synthesized materials have been evaluated as supercapacitor materials in 3M KOH using cyclic voltammetry (CV) at different potential scan rates and galvanostatic charge/discharge tests at different current densities. The FG-CoS electrodes showed a maximum specific capacitance of 1072 F/g at a scan rate of 1 mV/s and exhibited excellent cycling retention of 117% after 1000 cycles at 200 mV/s. The energy density was 35.2 Wh/kg with a power density of 250 W/kg at 1.0 A/g. Those figures of merit are much higher than those reported for graphene-based materials tested under similar conditions. The observed high performance can be related to the synergistic effects of CoS and 3-dimensional (3D) network crinkly sheets of functionalized spongy graphene.

Future Work:

Future work will include implementation of other metal sulphides incorporated with spongy reduced graphene oxide will be introduced such as MoS, RuS and NiS. In addition, Device measurement will be performed for the prepared composite in order to test the supercapacitor device in real life applications.